Master's thesis

NTNU
Norwegian University of Science and Technology
Faculty of Natural Sciences
Department of Chemical Engineering

Mikal Rekdal

Optimal Operation of a Solar Powered Thermal Energy Storage System for Cooking

Master's thesis in Chemical Engineering and Biotechnology

Supervisor: Johannes Jäschke

June 2020

NTNU
Norwegian University of
Science and Technology

Mikal Rekdal

Optimal Operation of a Solar Powered Thermal Energy Storage System for Cooking

Master's thesis in Chemical Engineering and Biotechnology
Supervisor: Johannes Jäschke
June 2020

Norwegian University of Science and Technology
Faculty of Natural Sciences
Department of Chemical Engineering

NTNU

Kunnskap for en bedre verden

Optimal Operation of a Solar Powered Thermal Energy Storage System for Cooking

TKP4900 - Chemical Process Technology, Master's Thesis

Mikal Rekdal

Supervisor: Prof. Johannes Jäschke
Co-supervisor: Prof. Ole Jørgen Nydal

Spring 2020

Norwegian University of Science and Technology
Department of Chemical Engineering

Abstract

In this thesis, the operation of a solar powered thermal energy storage system for cooking was modeled and optimized. The main objective was to investigate the potential cooking capacity of the system during varying conditions. A system prototype has been constructed at a laboratory at NTNU and in Arusha, Tanzania. The prototype consists of three tanks with oil that are heated by excess solar power and used as a heat transfer medium for cooking. A dynamic model was developed during the specialization project and modified during this work. Then, the cooking potential of the optimally operated system was studied by using model predictive control with the CasADi framework in MATLAB. The simulations suggest that the current physical system is sufficiently large to cook rice for 100 people when operated properly. By increasing the number of solar panels, the system is able to cook both for lunch and dinner during a day of sunny conditions. Other modifications to the physical system were also modeled, which indicated that a setup of two tanks is more energy efficient than the current three tank system.

Sammendrag

I denne masteroppgaven ble driften av et varmelagringssystem drevet av overskuddsenergi fra solcelleproduksjon for matlaging modellert og optimalisert. Hovedformålet med oppgaven var å undersøke systemets kapasitet under varierende forhold. En prototype av systemet har blitt konstruert på et laboratorium ved NTNU og i Arusha, Tanzania. Prototypen består av tre tønner med olje som varmes av overskuddsenergi og brukes som varmeoverføringsmedium for matlaging. En dynamisk modell av systemet ble utledet i fordypningsprosjektet og videreutviklet i dette masterprosjektet. Matlagingspotensialet under optimal drift ble videre undersøkt ved bruk av modellprediktivregulering med CasADirammeverket i MATLAB. Simuleringene antyder at det nåværende systemet er stort nok til å koke ris for 100 mennesker ved optimal regulering. Ved å øke antallet solcellepanel vil systemet være i stand til å lage mat både til lunsj og middag på en solrik dag. Andre modifiseringer på det fysiske systemet ble også modellert, som blant annet indikerte at et oppsett med to tanker er mer energieffektivt enn det nåværende tretanksystemet.

Preface

This master thesis was written in the spring of 2020 for the course TKP4900 - Chemical Process Technology, Master's Thesis. I would like to thank my supervisor, professor Johannes Jäschke and co-supervisor professor Ole Jørgen Nydal. Their help has been very valuable for me to complete my project. I feel lucky to have been working with a topic I am passionate about - making renewable energy even more accessible than it is today.

Finally, I am very grateful for having the opportunity of participating in the NORPART project. This gave me and fellow students the chance to experience Tanzania and the University of Dar es Salaam for a month during our work. The stay was both inspirational and fun, and just in time before the COVID-19 pandemic would have made the trip impossible!

Mikal Rekdal
Trondheim, Norway
15.06.2020

Contents

List of Figures

List of Tables

List of Symbols

A_{FR} Contact area between casserole and room [m^2]. 15, 23, 32

A_{PF} Contact area between cooking pan oil and casserole [m^2]. 15, 22, 32

A_{PR} Contact area between cooking pan oil and room [m^2]. 15, 22, 32

A_h Tank end area of section filled with liquid [m^2]. 20

A_{tank} Tank surface area [m^2]. 15, 17, 21, 24, 29, 51

A_v Cross-sectional area of manual valve opening [m^2]. 15, 19, 20, 32, 47

A Full tank end area [m^2]. 20

C_v Manual valve discharge coefficient [-]. 15, 19, 32, 47

Cp Heat capacity [J/kgK]. 6, 14, 16, 17, 21–24, 29, 32

D_{tank} Tank diameter [m]. 33, 35–37

F Filled volume fraction in tank [-]. 20, 21

L_{tank} Tank length [m]. 17, 33, 35–37

T_1 Temperature in tank 1 [K]. 14, 15, 17, 21, 35, 38, 39

T_2 Temperature in tank 2 [K]. i, xvi, xvii, 14, 15, 21, 22, 29, 35, 38–42, 44–46, 58

T_3 Temperature in tank 3 [K]. 14, 15, 17, 24, 35, 38, 39, 46

T_F Temperature in food [K]. 14, 15, 22, 23, 35, 38, 39, 42, 43, 46, 56

T_P Temperature in control volume P [K]. 14, 15, 22, 24, 35, 38, 39, 51

T_R Room temperature [K]. 15, 17, 18, 21–24, 29, 32

U Overall heat transfer coefficient [W/m^2K]. i, 15, 17, 21, 24, 29, 30, 32

V Full tank volume [m^3]. 20, 31, 33, 36, 51

$\Delta P_{friction}$ Frictional pressure drop [Pa]. 18, 19

ΔP_{valve} Manual valve pressure drop [Pa]. 19

$\hat{Q}_{1R}$ Heat loss from tank 1 [W]. 14, 15, 17

$\hat{Q}_{2R}$ Heat loss from tank 2 [W]. i, 14, 15, 18, 21, 29

$\hat{Q}_{3R}$ Heat loss from tank 3 [W]. 14, 15, 23, 24

$\hat{Q}_{FR}$ Heat loss from water in casserole [W]. 14, 15, 23, 31

$\hat{Q}_{PF}$ Heat transferred from pan to water [W]. 14, 15, 21–23, 31

$\hat{Q}_{PR}$ Heat loss from cooking pan [W]. 14, 15, 21–23

$\hat{Q}_{PV,max}$ Maximum available solar effect [W]. ii, iii, 13–15, 28, 29, 41–45, 59, 60

$\hat{Q}_{PV}$ Solar powered heating input used[W]. ii, iii, 14, 15, 18, 21, 33, 35, 36, 38–45, 47–49, 51, 57, 59

$\hat{Q}$ Heat flow [W]. 16, 17

$\hat{m}_{12}$ Mass flow from tank 1 to 2 [kg/s]. 14–16, 18, 21, 38, 39, 41–44

$\hat{m}_{2P}$ Mass flow from tank 2 to cooking pan [kg/s]. 14, 15, 18, 19, 21, 22, 26, 27, 33–36, 41, 44, 46, 47, 55, 57, 58

$\hat{m}_{31}$ Mass flow from tank 3 to 1 [kg/s]. 14–17, 23, 24, 41, 42

$\hat{m}_{P3}$ Mass flow from cooking pan to tank 3 [kg/s]. 14, 15, 18, 21, 23, 24

λ Failure rate [hr^{-1}]. 9, 52

ρ Density [kg/m^3]. 15, 18–20, 32, 47

θ Central angle [-]. 20, 21

g Acceleration of gravity [m/s^2]. 15, 18, 19, 32, 47

h_{12} Pipe height difference between tank 1 and 2 [m]. 32

h_{23} Pipe height difference between tank 2 and 3 [m]. 15, 18, 19, 32, 47

h_2 Liquid level height tank 2 [m]. 15, 18–20, 47

h_3 Liquid level height tank 3 [m]. 15, 18–20, 47

h_{FR} Heat transfer coefficient between casserole and room [W/m^2K]. 15, 23, 30–32

h_{PF} Heat transfer coefficient between cooking pan oil and casserole [W/m^2K]. 15, 22, 30–32

h_{PR} Heat transfer coefficient between cooking pan oil and room [W/m^2K]. 15, 22, 30–32

m Mass [kg]. 6, 16, 17, 20

r Tank radius [m]. 17, 20, 21

t_N Simulation time [s/min/hr]. 39, 41, 42, 44

u Control input [-]. 15, 16, 19, 20, 47

H Enthalpy [J/kgK]. 16, 17

m_1 Mass in tank 1 [kg]. 14, 16, 17, 35, 38, 39, 41, 42

m_2 Mass in tank 2 [kg]. 14, 18, 21, 29, 34–36, 38–41, 43–46, 48, 50, 57

m_3 Mass in tank 3 [kg]. 14, 24, 35, 36, 38, 39, 41–43, 46, 48

m_F Mass of food [kg]. 14, 23, 34, 35, 38, 39, 44–46

m_P Mass in cooking pan [kg]. 14, 22, 35, 38, 39

1 Introduction

A thermal energy storage system protoype has been assembled at the laboratories of the Department of Energy and Process Engineering at NTNU. The system uses excess solar power to heat palm oil that can be used as a heat source for cooking. In addition, a similar system has been set up in Arusha, Tanzania in order to perform field tests in realistic conditions. The system's purpose is to provide better indoor environment by replacing firewood with clean energy for cooking and store excess energy from solar power production for later use.

This thesis serves as an extension of the work done in the specialization project [1]. In the project, a mathematical model of the three tank system was developed. MATLAB scripts with an incomplete model were provided from the co-supervisor as a starting point. The main modification to the model was to develop the equations for the cooking unit, using basic principles of mass and energy balances. Simulations were designed to verify that the model behaved similarly to field tests. In this thesis, the model was adapted to the CasADi framework to establish optimal operation strategies for the physical system. In addition, scale-up possibilities and system modifications were designed to investigate potential energy efficiency improvements. Thus, the following objectives were established:

1. Improve the model equations and parameter accuracy developed in the project work.
2. Define realistic operational scenarios for the system. Decide objective functions and constraints for the given scenarios.
3. Optimize the system size required to cook for a given amount of people.
4. Study the system performance at varying weather conditions.
5. Investigate how different control strategies affect the energy efficiency.
6. Model potential designs for a larger scale system and compare energy efficiencies to the original system.
7. Calculate and compare the reliability of different large scale systems.
8. Model other modifications to the current system and study the change in performance.

1.1 Motivation

The increasing world population is matched by a growing demand for energy. BP's annual review of world energy reported that the global primary energy consumption grew by 2.9 % in 2018. The year also experienced the highest growth rate of carbon emissions from energy production since 2010/2011 [2]. These rates show an increasing gap between emissions and joint international efforts of reducing climate impact. However, 2018 was also a year for growth in renewable energy supply. The production grew by 14.5 % accounting for 9.3 %

of the total power generation. Although this shows a promising development, BP's report emphasises that the transition to renewable sources must happen faster to reach the Paris climate goals [2].

Renewable energy sources such as wind and solar power offer lower emissions than their fossil fuel counterparts. Wind and solar power are the fastest growing renewable sources globally and are rapidly emerging technologies in many regions of the world [2]. The energy can be harvested in both small and large scale systems, offering flexibility to regions with lacking infrastructure. However, a major challenge with solar and wind are their variable energy supply. For instance, during cloudy periods, the effect of PV panels drastically drops and reaches zero production during dark hours. For an area completely dependant on solar power without storage capabilities, this means that cooking or using light in the evening becomes impossible.

In Central, East, Southern and West Africa, cooking accounts for nearly 80% of residential energy consumption. These areas often depend on firewood for cooking. The use of traditional biomass stoves pose both health and economic issues. Approximately 600 000 people die each year in these regions from exposure to toxic fumes. In addition, economic implications include hours spent on collecting biomass and inefficient cooking [3]. An example of settlements facing these challenges is refugee camps, where people struggle with cooking food rations properly and efficiently. For instance, Barbieri et.al. (2017) reported that in Niger, rations in refugee camps have largely been consumed dry or in some cases using water that has not been boiled. The reason was that cooking was time-consuming and required a large amount of fuels. This is problematic because it can lead to less nutritional value or increase risks of infection in case of improperly preparing the food [4]. Providing these areas with simple cooking methods using clean energy is therefore likely to increase quality of life.

In order to mitigate the variability of renewable energy production, power can be stored when the generated supply is higher then the demand. The stored energy then acts as a buffer to utilize the excess energy when power is not generated. There are several technologies available for storing produced renewable electricity. They store electrical energy in other electrical, thermal, chemical, mechanical or electrochemical forms. The choice of medium depends on a number of factors such as the required storage time, capacity, applications and cost. The main purpose is to increase the reliability and robustness of the power supply [5].

1.2 Previous Work and Project Contribution

Off-grid systems typically charge batteries when the power production is larger than the demand. When the capacity of the battery is full, the excess energy is usually dumped as heat, by passing the current through a resistor. An optimization model for an off-grid PV system was described by Sandwell et.al. (2016), where parts of the excess energy are stored in batteries. However, a significant production of the electricity is lost, which can be considered wasted energy [6].

One way of storing the excess energy is by thermal energy storage systems. The excess energy is directed to a medium where the heat is stored rather than dumped. Water is commonly used as storage material, due to its availability, low cost and high heat capacity [7]. In the physical pilot for this project, palm oil is used as storage medium. Thaule et.al. (2019) points out that a temperature of about 100 °C is desired for cooking. Thus, a medium that can hold a temperature of 100 - 250 °C is desirable. As thermal oils and edible oils have a higher boiling point than water, this makes them more suitable for high temperature energy storage [8].

In order to utilize as much of the stored energy as possible, it is often of interest to optimize the operation of thermal energy storages. Several optimization techniques are being used for various storage systems, as described in the review by Ooka et. al. (2019). Mathematical techniques such as mixed integer linear programming (MILP) and dynamic programming (DP) are highlighted as precise techniques that can obtain exact solutions, given that the required information is available and accurate [7].

In this project, the mathematical technique of nonlinear programming (NLP) was used to optimize the model, which is further described in the chapters 2 and 4. The model was derived using well-known mass and heat transfer equations from literature, described in chapter 3. As mentioned, there have been several studies on modeling and optimizing thermal energy storage systems. The novelty of this thesis lies in having created a specific model to investigate optimal operation of the unique thermal energy storage system at NTNU. Additionally, new designs were simulated to investigate the performance of other new prototypes before building physical systems.

1.3 Thesis Structure

This thesis is divided into six chapters. In chapter 2, relevant background theory for the project is discussed. This includes thermal energy storage, optimization and reliability theory. Chapter 3 introduces the physical system, the model and a detailed derivation of the equations. In chapter 4, the tools used are presented. Then, the six case studies

created are described, with their respective optimization problems presented in detail. The case studies were designed to answer the final six objectives listed previously. Results of importance are selected to reflect findings of importance and the presentation thus varies between studies. In addition, a discussion of the results and their significance are included. Chapter 5 discusses other important aspects of the work and suggestions for further work, while chapter 6 summarizes key findings.

2 Theory

The theory introduces elements of thermal energy storage technology that are relevant to the physical system. Then, the mathematical optimization techniques used in the project are introduced. Finally, system reliability theory is introduced, which was applied when considering a scale-up of the system.

2.1 Thermal Energy Storage

The main purpose of a thermal energy storage (TES) system is to mitigate the mismatch between energy supply and demand. Generally, the storage system repeats a cycle of three steps: charge, storage and discharge, as illustrated in figure 2.1. When energy is abundant or cheap, a storage medium is charged using excess energy. The storage medium must be able to retain the energy for a shorter or longer period of time, depending on the application. As the demand exceeds the supply, energy is discharged from the storage. The technology is especially relevant for renewable energy sources of variable supply such as wind and solar power generation [9].

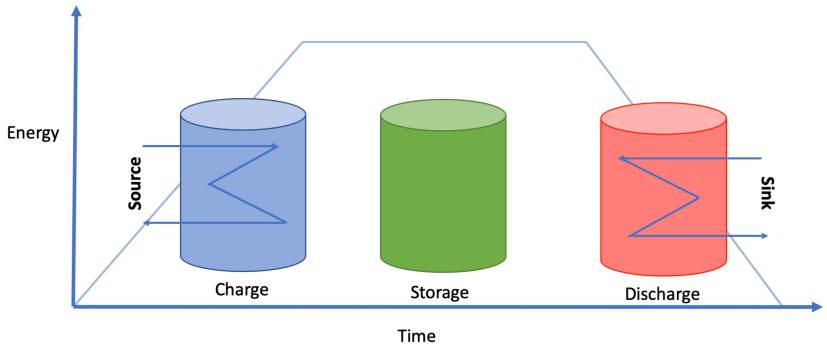

Figure 2.1: A generic thermal energy storage cycle over time. The system is charged by the source or drained to the sink, depending on energy pricing or availability.

Thermal energy storage can be divided into latent and sensible thermal energy. Latent energy storage uses phase changing materials to store the heat as the material changes phase. In sensible thermal storage, the temperature of the storage medium is either raised or lowered to store or extract heat. The choice of technology depends on a variety of factors such as the required storage period, costs and operating conditions [10]. The system in question for this project uses sensible storage, which is therefore further discussed below.

Sensible energy thermal storage systems change the temperature of the storage medium by the input or output of heat. The amount of energy stored, Q, is defined by the following equation

$$Q = mCp\Delta T \tag{2.1}$$

where m is the mass of the storage medium, Cp its heat capacity and ΔT the change in temperature of the medium. Commonly used storage mediums include solids such as bricks or concrete, and liquids such as water or molten salts. Solids have the advantage of high specific heat capacities, allowing for compact storage. Liquids are often advantageous when it is of interest to pump and transport the storage medium. They also typically provide higher heat transfer rates than solids [10], [11].

2.2 Optimization

The task of optimization is relevant in most engineering applications. A method is developed to perform decision-making in a systematic and and efficient way. Optimization can be described as finding the best solution to a problem within any defined constraints. The constraints can include both feasibility conditions and process requirements. An example is an open water tank that is not allowed to boil or freeze. A water volume that is negative or higher than the tank violates the laws of physics, thus they are feasibility conditions. Keeping the temperature between 0 °C and 100 °C is physically possible, but specified as undesirable, making them process requirements.

The optimization problem consists of three parts: the objective function, the model and constraints. The objective function is a scalar that needs to be maximized or minimized. The function is a measurement of the system's performance in terms of cost, efficiency, yield or similar expressions. The model describes the behavior of the system in terms of equality and inequality equations. The model thus defines the constraints and behavior of the system. The variables in the model are adjusted to satisfy the constraints, while minimizing or maximizing the objective function [12].

The most general form of a continuous optimization problem is a nonlinear program (NLP) which has the form below

$$\begin{aligned} &\min_{x(t)} \ f(x(t)) \\ &s.t. \ h(x(t)) = 0 \\ &g(x(t)) \leq 0 \end{aligned} \tag{2.2}$$

Here, $f(x(t))$ is the objective function, $h(x(t))$ are equations describing the behavior of the model and $g(x(t))$ are inequality or equality constraints for specifications or requirements

of the system. $x(t)$ is the variable that is adjusted to optimize the objective function.

2.2.1 Model Predictive Control

Model Predictive Control (MPC) is a technique that uses optimization as a tool for implementing optimal control strategies [12]. The technique uses a process model to predict the future behavior of the system. The process model can be linear and derived from empirical system identification. Alternatively, the model is mathematically derived with a set of differential algebraic equations (DAEs). Any relevant process constraints must also be defined. MPC allows constraints on both input and output variables as well as allowing for multivariable control. In practice, model predictive control consists of the following steps, illustrated in figure 2.2 [13]:

1. The current system states are measured.
2. The trajectory is optimized over a given time horizon, called the prediction horizon, N_p.
3. The first predicted input, u, is implemented until the next time interval.
4. The horizon is shifted to the next interval where the three previous steps are repeated.

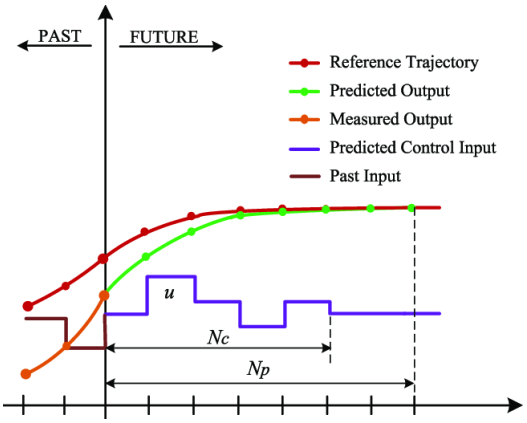

Figure 2.2: Illustration of model predictive control. Illustration from [13].

2.2.2 Direct Multiple Shooting Method

One method of solving the dynamic optimization problem is by using the direct multiple shooting approach. Here, the time horizon is divided into control intervals called shooting intervals. The DAE models are integrated separately in each time interval, such as from time t_k to t_{k+1} in figure 2.3 below. The integration for this interval starts with x_k and is integrated to $\tilde{f}(x_k, u_k)$. The states are now added as decision variables in the problem, in addition to the control input, u_k. The state trajectories must be continuous, so a shooting gap is also added as a constraint for the problem.

$$x_{k+1} - \tilde{f}(x_k, u_k) = 0 \ \forall \ k \ \in 1, ..., N \tag{2.3}$$

The method can handle nonlinear and unstable problems very well, due to short integration intervals. This limits the time frame of the model to reach unstable domains. In addition, as the states are decision variables, state constraints are imposed at the end of each shooting interval. This confines the states to a bounded region. A disadvantage of the method is that the optimization problem becomes large. Instead of using only control inputs as decision variables, both control inputs and state variables are used to solve the problem [12].

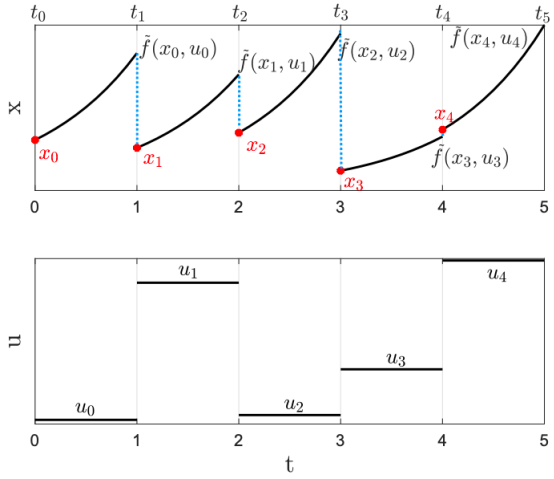

Figure 2.3: Illustration of the multiple shooting method from [14]. System states are integrated in separate intervals. Both control inputs and system states are used as decision variables. Constraints are imposed to ensure continuous behavior between the intervals.

2.3 Reliability Theory

Reliability can be defined as the probability that an item or system performs its required function, given a specified environment and period of time [15]. The reliability at time t, is the probability that the time of failure for the component, T, is larger than time t, as seen in equation 2.4. The reliability of the system is complementary to the probability of failure before time t by the following relation

$$R(t) = P(T > t) = 1 - F(t) \tag{2.4}$$

where $F(t)$ is the distribution function of failure at time t.

2.3.1 Failure Functions

A component's time to failure is the time it takes for a component to fail for the first time. The probability distribution can take on many forms, such as the normal distribution, gamma distribution and exponential distribution. Often, the distribution is determined empirically for a component. The exponential distribution is the most used in applied reliability analysis, due to its mathematical simplicity and realistic lifetime distribution for some items [15].

An exponential failure distribution density function takes the following form:

$$f(t) = \begin{cases} \lambda e^{-\lambda t} & \text{for } t > 0, \lambda > 0 \\ 0 & \text{otherwise} \end{cases} \tag{2.5}$$

where λ is the constant failure rate per time unit, usually experimentally determined. For an exponential distribution, the reliability is therefore

$$R(t) = 1 - F(t) = 1 - \int_0^t f(u)du = e^{-\lambda t} \tag{2.6}$$

2.3.2 k-out-of-n Structure

Many systems have redundant components as a safety measure to increase the reliability. This is called a k-out-of-n ($koon$) structure, where k components must function out of all n components for the system to work. This ensures that the system can operate even if one or several components of the system breaks down. An example is illustrated below for a 2oo3 (2-out-of-3) structure in figure 2.4. There are three minimal working structures where one system component has failed. As the three configurations are in parallel, all three configurations ensure that the system works. However, if a second component breaks, all three series structures are broken, and the system cannot function properly.

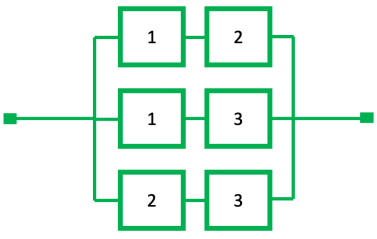

Figure 2.4: The three minimal working structures for a 2oo3 system. The system requires that at least two of the three components function for the system to function.

The reliability of a $koon$ system with equal failure probabilities of each component has a binomial distribution. If the reliability of each component is $r(t)$, the reliability of the system R_s(t), is

$$R_s(t) = \sum_{x=k}^{n} \binom{n}{x} r(t)^x (1 - r(t))^{n-x} \tag{2.7}$$

3 System Modeling

In this chapter, the physical system is introduced. The assumptions and resulting model equations for the system are then presented. A stepwise derivation of the model is also included, with the derivation of subchapters 3.4 - 3.8 being largely a part of the project work. The text is included because the heat transfer equations have been altered from the project work, and so that the thesis can be read independently of the project report. Finally, the additional modeling work new to this thesis is presented. This includes the description of the alternative system configurations, the modeled weather variations and heat transfer coefficients estimations.

3.1 System Description

The assembled system at the NTNU laboratory is shown below in figure 3.1, with its components described in table 3.1. The key components of the system are more clearly illustrated in figure 3.2.

Figure 3.1: Overview of the system at NTNU, with labels described in table 3.1. The prototype in Arusha has replaced the frying pan (9) with a larger cooker (8). The picture and table 3.1 are reproduced from reference [8].

Table 3.1: System parts of figure 3.1.

Number	Part
1	Tank 1
2	Tank 2 (storage)
3	Tank 3
4	PicoLogger
5	Power supply cables to heating elements
6	Hand pump
7	Hose to flush pan
8	Cooker
9	Frying pan
10	Tray for spilling
11	Valve to tank 1
12	Valve to frying pan

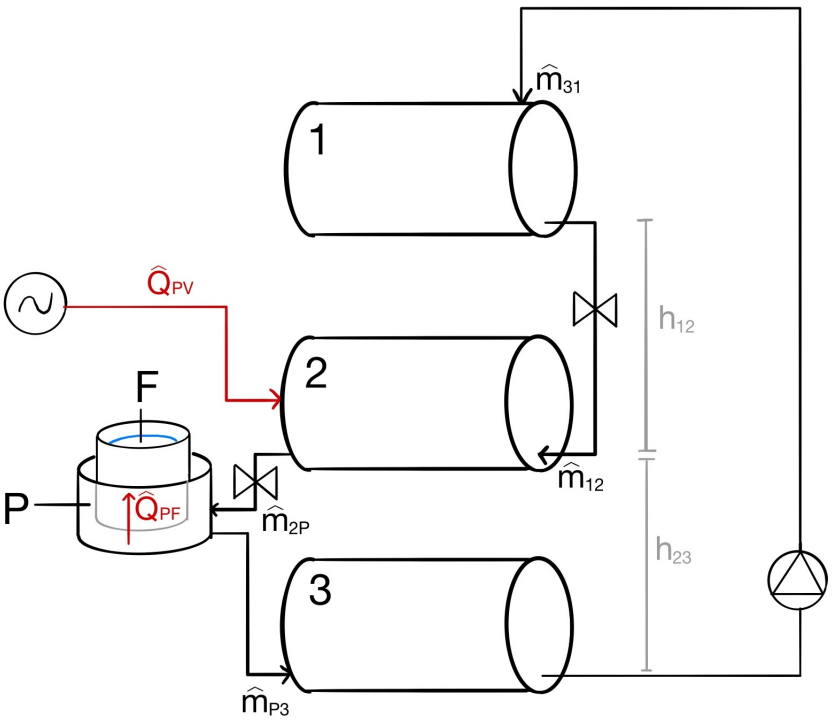

Figure 3.2: Illustration of the main features of the system. Heat transfers are illustrated by red arrows, while black arrows represent mass transfers. An additional heat loss to the environment is modeled from each control volume, but not depicted here.

The system consists of three tanks containing oil, shown as control volumes 1, 2 and 3 in figure 3.2. The tanks are arranged vertically, with a gravity driven oil flow from top to bottom. Electrical heating elements are placed in tank 2 to heat up the oil, powered by solar

panels. Note that the second tank is called tank 2 and the storage tank interchangeably throughout the text. The flow from tank 1 to tank 2 is controlled by a thermostatic valve that controls the maximum temperature in tank 2. Consistent with the system setup in Arusha, only a cooker was considered for preparing the food. The frying pan of the NTNU system is therefore not discussed further. A manually operated valve is installed between tank 2 and the cooking pan. Opening the valve allows the flow of hot oil through the cooking pan, denoted control volume P, where a casserole containing water is placed. As the hot oil flows through the pan, the casserole and water/food inside, named control volume F, is heated. Hot oil exits the cooking pan and accumulates in tank 3. The system is a closed loop, with a manual pump installed to pump oil from tank 3 up to tank 1.

The main difference between the physical model and simulation model lies in the control behavior of the valve between tank 2 and the cooking pan. The simulations will mainly consider scenarios where the mass flow is controlled directly. This behavior is similar to a thermostatic valve, rather than the manually operated valve of the physical system. The alteration was done to investigate the effect of replacing the manual valve with a thermostatic valve to operate closer to optimal control.

3.2 Assumptions

In establishing a model of the system, the following assumptions were made

1. The oil is well mixed in all flows and control volumes, giving a uniform temperature.
2. The water is well mixed in the casserole with a uniform temperature.
3. The heat capacity of the water and oil is constant.
4. The densities of the water and oil are constant.
5. Pipes are well isolated, resulting in negligible heat loss.

The two first simplifications were considered valid as liquids generally have high heat transfer rates [9]. The three latter points were identified as more important simplifications as they directly affect the storage capacity of the system. The assumptions are therefore elaborated on in chapter 5. Additional assumptions for specific control volumes are explained in the model derivation.

3.3 Equations Summary

The established model is given in tables 3.2 - 3.3. The system has ten states of interest, which is the mass and temperature of each control volume, as shown in table 3.2. There is one disturbance, $\hat{Q}_{PV,max}$, which is the maximum available solar effect, dependant on weather conditions. Modeling of $\hat{Q}_{PV,max}$ is discussed towards the end of the chapter. The

system was optimized using five control inputs. Firstly, the solar input used, $\hat{Q}_{PV}$, of total solar energy available, $\hat{Q}_{PV,max}$. Additionally, the three mass flows $\hat{m}_{12}$, $\hat{m}_{2P}$ and $\hat{m}_{31}$ were flow controlled. Finally, a manual valve opening control of $\hat{m}_{2P}$ was considered in case study 3, where the valve opening is optimized, rather than the mass flow directly.

Table 3.2: Differential equations for the ten system states.

States	Description	Equation
$\dot{T}_1$	Tank 1 temperature	$\dot{T}_1 = \frac{1}{m_1}(\hat{m}_{31}(T_3 - T_1) - \frac{\hat{Q}_{1R}}{Cp_{oil}})$
$\dot{T}_2$	Tank 2 temperature	$\dot{T}_2 = \frac{1}{m_2}(\hat{m}_{12}(T_1 - T_2) + \frac{\hat{Q}_{PV}}{Cp_{oil}} - \frac{\hat{Q}_{2R}}{Cp_{oil}})$
$\dot{T}_P$	Cooking pan temperature	$\dot{T}_P = \frac{1}{m_P}(\hat{m}_{2P}(T_2 - T_P) - \frac{\hat{Q}_{PF}}{Cp_{oil}} - \frac{\hat{Q}_{PR}}{Cp_{oil}})$
$\dot{T}_F$	Food temperature	$\dot{T}_F = \frac{1}{m_F Cp_{water}}(\hat{Q}_{PF} - \hat{Q}_{FR})$
$\dot{T}_3$	Tank 3 temperature	$\dot{T}_3 = \frac{1}{m_3}(\hat{m}_{P3}(T_P - T_3) - \frac{\hat{Q}_{3R}}{Cp_{oil}})$
$\dot{m}_1$	Tank 1 mass	$\dot{m}_1 = \hat{m}_{31} - \hat{m}_{12}$
$\dot{m}_2$	Tank 2 mass	$\dot{m}_2 = \hat{m}_{12} - \hat{m}_{2P}$
$\dot{m}_P$	Cooking pan oil mass	0
$\dot{m}_F$	Food mass	0
$\dot{m}_3$	Tank 3 mass	$\dot{m}_3 = \hat{m}_{P3} - \hat{m}_{31}$

Table 3.3: Control inputs of the system.

Value	Description	Equation	Range	Unit
$\hat{Q}_{PV}$	Solar input to the system	u_1	0 - $\hat{Q}_{PV,max}$	W
$\hat{m}_{12}$	Mass flow tank 1 to 2	u_2	0 - 1.0	kg/s
$\hat{m}_{2P}$	Mass flow tank 2 to pan, thermostat	u_3	0 - 1.0	kg/s
	Mass flow tank 2 to pan, manual	$\rho \sqrt{\frac{2g(h_2 - h_3 + h_{23})}{\frac{1}{(C_v \cdot u_5 \cdot A_{v0})^2}}}$	0 - 1.0	-
$\hat{m}_{P3}$	Mass flow pan to tank 3	$\hat{m}_{2P}$	0 - 1.0	kg/s
$\hat{m}_{31}$	Mass flow tank 3 to 1	u_4	0 - 1.0	kg/s

Table 3.4: Heat transfer equations of the system.

Value	Description	Equation
$\hat{Q}_{1R}$	Heat loss tank 1 to room	$\hat{Q}_{1R} = UA_{tank}(T_1 - T_R)$
$\hat{Q}_{2R}$	Heat loss tank 2 to room	$\hat{Q}_{2R} = U_2 A_{tank}(T_2 - T_R)$
$\hat{Q}_{PF}$	Heat transfer cooking pan to food	$\hat{Q}_{PF} = h_{PF} A_{PF}(T_P - T_F)$
$\hat{Q}_{PR}$	Heat loss cooking pan to room	$\hat{Q}_{PR} = h_{PR} A_{PR}(T_P - T_R)$
$\hat{Q}_{FR}$	Heat loss food to room	$\hat{Q}_{FR} = h_{FR} A_{FR}(T_F - T_R)$
$\hat{Q}_{3R}$	Heat loss tank 3 to room	$\hat{Q}_{3R} = UA_{tank}(T_3 - T_R)$

3.4 Tank 1

Three flows are considered in the control volume of tank 1. There is the mass and enthalpy inflow from tank 3 to 1, $\hat{m}_{31}$, the outflow from tank 1 to tank 2, $\hat{m}_{12}$, and the heat loss from tank 1 to the room, $\hat{Q}_{1R}$. The flows are marked in figure 3.3 below

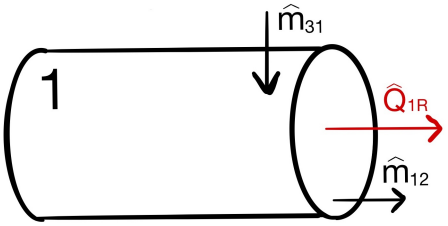

Figure 3.3: Mass and energy in- and outflows of tank 1.

3.4.1 Mass Balance

The accumulation of mass in the control volume, $\dot{m}_1$, can be described as the difference between in- and outflows, here $\hat{m}_{31}$ and $\hat{m}_{12}$ respectively

$$\dot{m}_1 = \hat{m}_{31} - \hat{m}_{12} \tag{3.1}$$

The inflow is set by the pumping rate u_4, which is an input to the system by operating the manual hand pump

$$\hat{m}_{31} = u_4 \tag{3.2}$$

In the case studies considered, the mass flow from tank 1 to tank 2, $\hat{m}_{12}$, was modeled as a control input as shown in equation 3.3.

$$\hat{m}_{12} = u_2 \tag{3.3}$$

3.4.2 Energy Balance

With the mass flows fully described, it is possible to develop the energy balance and temperature of tank 1. The general enthalpy balance for the control volume, assuming negligible pressure-volume work and shaft work, can be described by

$$\dot{H} = \sum \hat{H}_{in} - \sum \hat{H}_{out} + \hat{Q}_{net} \tag{3.4}$$

$\dot{H}$ is the change in enthalpy with respect to time, $\hat{H}_{in}$ and $\hat{H}_{out}$ are the enthalpy flows in and out of the control volume and $\hat{Q}_{net}$ is heat added through the wall [16].

The enthalpy, H, is described by

$$H(T) = H(T_{ref}) + m \int_{T_{ref}}^{T2} Cp(T)dT \tag{3.5}$$

where Cp is the heat capacity of the substance and $H(T_{ref})$ is the enthalpy at the reference temperature, T_{ref}. To evaluate the change in temperature in control volume i, $\dot{T}_i$, the enthalpy expression can be expanded, assuming that the heat capacity is independent of temperature and thus time

$$\dot{H}_i = \frac{d}{dt}(m_i Cp T_i) = \hat{m}_{in} Cp T_{in} - \hat{m}_{out} Cp T_{out} + \hat{Q}_{net} \tag{3.6}$$

and re-arranged

$$Cp(\dot{m}_i T_i + \dot{T}_i m_i) = \hat{m}_{in} Cp T_{in} - \hat{m}_{out} Cp T_{out} + \hat{Q}_{net} \tag{3.7}$$

Here, $T_{out} = T_i$ and $\dot{m}_i = \hat{m}_{in} - \hat{m}_{out}$ so the temperature change is expressed by

$$\dot{T}_i = \frac{1}{m_i}(\hat{m}_{in}(T_{in} - T_i) + \frac{\hat{Q}_{net}}{Cp}) \tag{3.8}$$

For tank 1, the only heat transfer considered is heat loss from the tank surface to the room, $\hat{Q}_{1R}$. Thus, the following expression is found for tank 1

$$\dot{T}_1 = \frac{1}{m_1}(\hat{m}_{31}(T_3 - T_1) - \frac{\hat{Q}_{1R}}{Cp_{oil}}) \tag{3.9}$$

3.4.3 Heat Transfer

The heat loss is assumed to be uniform over the surface area of the tank. Thus, the area of heat loss of the cylindrical tank is

$$A_{tank} = 2\pi r^2 + 2\pi r L_{tank} \tag{3.10}$$

where r is the radius of the tank and L_{tank} the tank length.

It was assumed that the convective heat loss $\hat{Q}_{1R}$ follows Newton's law of cooling. The law states that the rate of heat loss is proportional to the difference in temperature between the body and its surroundings [17]

$$\hat{Q}_{1R} = U A_{tank}(T_1 - T_R) \tag{3.11}$$

where U is the overall heat transfer coefficient, assumed to be independent of temperature

and T_R is the room temperature.

3.5 Tank 2

In tank 2, two mass streams are considered. These are the inflow from tank 1, $\hat{m}_{12}$, and the outflow to the cooking plate, $\hat{m}_{2P}$. Additionally, two heat transfers are considered. These are the input of the heating elements, $\hat{Q}_{PV}$ and heat loss to the room, $\hat{Q}_{2R}$. All four flows are indicated in figure 3.4

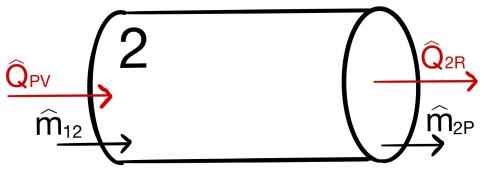

Figure 3.4: Mass and energy in- and outflows of tank 2.

The differential mass balance for tank 2 is

$$\dot{m}_2 = \hat{m}_{12} - \hat{m}_{2P} \tag{3.12}$$

$\hat{m}_{12}$ is already expressed by equation $\hat{m}_{12}$, while $\hat{m}_{2P}$ must be derived. In the majority of the case studies, the mass flow was controlled directly like $\hat{m}_{12}$, as shown in equation 3.20b. However, the current system relies on manual opening of a valve between tank 2 and the cooking pan. Therefore, an expression for the dynamic mass flow as a function of valve opening was derived.

The volume of control volume P is small compared to the three tanks. It was assumed to contain a constant mass, and that the flow quickly reached steady state. This means that the mass flow into P, $\hat{m}_{2P}$ is equal to the outflow of P, $\hat{m}_{P3}$

$$\hat{m}_{2P} = \hat{m}_{P3} \tag{3.13}$$

The mass flow from tank 2 to 3 is gravity driven. The flow passes through the pipe, cooking pan and manual valve. Thus, the opening of the valve to the cooking pan limits the flow. For calculating the flow, it was assumed that there is a steady state balance between the pressure difference of the tanks and the friction loss. In other words

$$\rho g(h_2 + h_{23} - h_3) = \Delta P_{friction} \tag{3.14}$$

where h_2 and h_3 are the liquid levels in tank 2 and 3 and g is the standard acceleration of gravity. h_{23} is the height difference between the outlet of tank 2 and inlet of tank 3, depicted in figure 3.2. Due to the short length of the pipes, it was assumed that this pipe friction contribution was negligible. The friction loss, $\Delta P_{friction}$, is then due to flow through the manually operated valve, ΔP_{valve}. Rewriting of equation 3.14 gives

$$\rho g \Delta h_2 = \Delta P_{valve} \tag{3.15}$$

Where

$$\Delta h_2 = h_2 + h_{23} - h_3 \tag{3.16}$$

The flow across the valve was modeled by a typical valve equation

$$\hat{m}_{2P} = C_v A_v \sqrt{2\rho \Delta P_{valve}} \tag{3.17}$$

with C_v being the discharge coefficient and A_v the area of the valve opening.

Rearranging equation 3.17 and solving for pressure drop across the valve gives

$$\Delta P_{valve} = \frac{{\hat{m}_{2P}}^2}{(C_v A_v)^2 2\rho} \tag{3.18}$$

Thus, the following relation is established combining equation 3.15 and equation 3.18

$$\rho g \Delta h_2 = \frac{{\hat{m}_{2P}}^2}{2\rho} \left(\frac{1}{(C_v A_v)^2}\right) \tag{3.19}$$

Solving for the mass flow, $\hat{m}_{2P}$ is calculated as shown in equation 3.20a.

$$\hat{m}_{2P} = \rho \sqrt{\frac{2g(h_2 - h_3 + h_{23})}{\frac{1}{(C_v A_v)^2}}} \tag{3.20a}$$

$$\hat{m}_{2P} = u_3 \tag{3.20b}$$

Three variables are missing before the mass flow in equation 3.20a can be calculated. These are A_v, by adjusting the valve opening and the liquid levels in tanks 2 and 3, h_2 and h_3.

3.5.1 Temperature Control

The area of the open manual valve was assumed to be linear with opening fraction, u_5. The cross-sectional opening area of the opening hole, A_v, is then

$$A_v = A_{v0}u_5 \tag{3.21}$$

where A_{v0} is the area of a fully open valve.

3.5.2 Liquid Level

h_2 and h_3 can be found using geometric arguments. Beginning with the volume fraction of the tank occupied, F, calculated as

$$F = \frac{m}{\rho V} \tag{3.22}$$

with ρ being the density of the liquid, m the mass in the tank and V the volume of a full tank.

The tank end area of the liquid section, A_h, is a fraction of the total tank end area, expressed as

$$A_h = F\pi r^2 \tag{3.23}$$

where r is the radius of the tank. Another expression for A_h can be found using the central angle, θ, illustrated below in figure 3.5

$$A_h = \frac{1}{2}r^2(\theta - sin(\theta)) \tag{3.24}$$

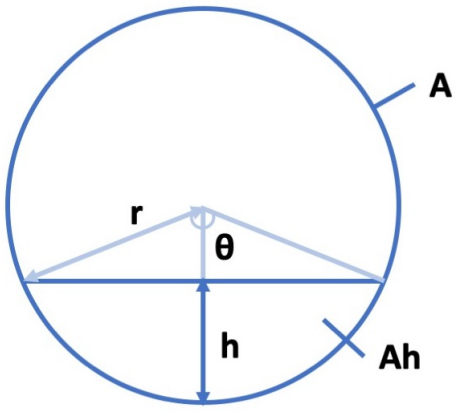

Figure 3.5: End dimensions of a partially filled cylindrical tank. A is the total area of the tank end, while A_h is the area of the tank end up to the filled liquid level h.

Combining equation 3.23 and equation 3.24, the following expression is obtained

$$\theta - sin(\theta) = 2\pi F \tag{3.25}$$

which can be used to solve θ implicitly.

Then, the level in the tank, h, can be calculated by the radius of the tank, r, and θ as follows

$$h = r(1 - cos(\frac{\theta}{2})) \tag{3.26}$$

The liquid level height of tank 2 is calculated using the same geometric arguments. Now, the mass transport $\hat{m}_{2P}$ is only expressed in known variables and can be calculated.

The expression for the energy balance is quite similar as for tank 1. A heat loss from tank 2 to the room, $\hat{Q}_{2R}$, is also considered here. In addition, tank 2 has a heating input, $\hat{Q}_{PV}$, giving the following expression

$$\dot{T_2} = \frac{1}{m_2}(\hat{m}_{12}(T_1 - T_2) + \frac{\hat{Q}_{PV}}{Cp_{oil}} - \frac{\hat{Q}_{2R}}{Cp_{oil}}) \tag{3.27}$$

$\hat{Q}_{PV}$ is the delivered effect of the heating elements powered by solar panels. The heat loss to the room is assumed to follow the behavior of tank 1, giving

$$\hat{Q}_{2R} = U_2 A_{tank}(T_2 - T_R) \tag{3.28}$$

A significantly lower heat transfer coefficient value was used for tank 2 compared to 1 and 3 due to more insulation around this tank in the physical system.

3.6 Cooking Pan

In this model, a cooking pan is used for preparing food, consistent with the system in Arusha. Oil flows from tank 2 to the pan, which is a container of hot oil. The oil exits from the other side of the pan in mass stream $\hat{m}_{P3}$. Two heat transfers are associated with the control volume of oil, as shown in figure 3.6. These are a heat loss to the room,$\hat{Q}_{PR}$, and heat utilized to cook food, $\hat{Q}_{PF}$.

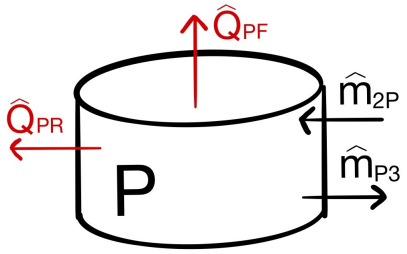

Figure 3.6: Mass and energy in- and outflows of the oil bath in the cooking pan.

Due to the assumption of steady state flow as stated in equation 3.13, the mass is constant in the pan

$$\dot{m_P} = 0 \tag{3.29}$$

The expression for the temperature is then

$$\dot{T_P} = \frac{1}{m_P}(\hat{m}_{2P}(T_2 - T_P) - \frac{\hat{Q}_{PF}}{Cp_{oil}} - \frac{\hat{Q}_{PR}}{Cp_{oil}}) \tag{3.30}$$

For $\hat{Q}_{PF}$, it is assumed that an overall heat transfer coefficient can be found for the heat transfer through the metal casserole to the water. It is also assumed that the casserole is partly submerged in oil. This contact area between the casserole and oil, A_{PF}, was considered as the significant heat transfer area. The heat transferred from the hot oil to the water is then

$$\hat{Q}_{PF} = h_{PF}A_{PF}(T_P - T_F) \tag{3.31}$$

with h_{PF} being the heat transfer coefficient through the casserole. The heat loss directly from the oil in the cooking pan to the room, $\hat{Q}_{PR}$, depends on various factors. The container is highly insulated and was assumed to have negligible heat loss. Thus the heat loss was modeled from the oil that is directly exposed to air, which depends on the submerged casserole's size. The heat loss was estimated with the area of oil in the cooking pan exposed to air, A_{PR}, as well as an estimated heat transfer coefficient, h_{PR}

$$\hat{Q}_{PR} = h_{PR}A_{PR}(T_P - T_R) \tag{3.32}$$

3.7 Food in Casserole

Only the mass of water is considered in evaluating the enthalpy and temperature in the casserole. The addition of food, for instance rice, is assumed to have negligible effect on the mass and heat capacity in control volume F. Thus, the time water was kept at boiling point was considered cooking time. The casserole is likely to have a lid on to limit heat loss to the environment. The mass inside the casserole is then constant, without water evaporation

$$\dot{m_F} = 0 \tag{3.33}$$

For control volume F, shown in figure 3.7, the two flows to consider are therefore the heat loss to the room,$\hat{Q}_{FR}$, and the heat transfer from the pan, $\hat{Q}_{PF}$.

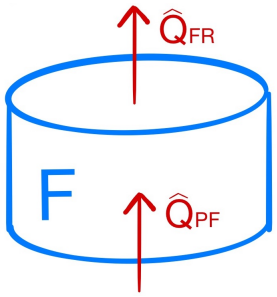

Figure 3.7: Energy in- and outflows of the water/food in the casserole.

The energy balance for the water was therefore modeled as

$$\dot{T_F} = \frac{1}{m_F C p_{water}}(\hat{Q}_{PF} - \hat{Q}_{FR}) \tag{3.34}$$

Like $\hat{Q}_{PR}$, the heat loss from the water to the room, $\hat{Q}_{FR}$, depends on numerous factors such as the size and material of the casserole. The heat loss was modeled as the heat transfer from the part of the casserole exposed to the room, A_{FR}, with an overall heat transfer coefficient, h_{FR}

$$\hat{Q}_{FR} = h_{FR} A_{FR}(T_F - T_R) \tag{3.35}$$

3.8 Tank 3

Tank 3 also has a heat loss to the room, $\hat{Q}_{3R}$, as well as the in and out flows $\hat{m}_{P3}$ and $\hat{m}_{31}$, shown in figure 3.8

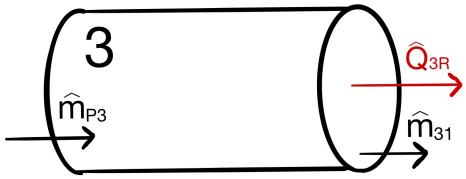

Figure 3.8: Mass and energy in- and outflows of tank 3.

The accumulation of m_3 is described by the in and out flows of discussed in equations 3.2 and 3.13

$$\dot{m_3} = \hat{m}_{P3} - \hat{m}_{31} \tag{3.36}$$

Giving the following change in temperature

$$\dot{T_3} = \frac{1}{m_3}(\hat{m}_{P3}(T_P - T_3) - \frac{\hat{Q}_{3R}}{Cp_{oil}}) \tag{3.37}$$

Like the other tanks, an equivalent heat loss expression has been established

$$\hat{Q}_{3R} = UA_{tank}(T_3 - T_R) \tag{3.38}$$

3.9 Other Design Configurations

The three first case studies considered the developed model presented so far. Several other designs differing from the physical system were also modeled to investigate possibilities of scale-up or improving system energy efficiency. All of the systems introduced below are re-configurations of the five key elements: Tank 1, tank 2, tank 3, the cooking pan and food in the casserole. Thus, each individual control volume was modeled as introduced previously unless otherwise stated.

3.9.1 Large Scale System

As a base case, the system was sized to cook 100 portions of rice. In order to cook for a total of 500 people, two configurations were considered. One option considered was to construct five standalone systems identical to the current one, with each scaled to cook for 100 people, as shown below in figure 3.9.

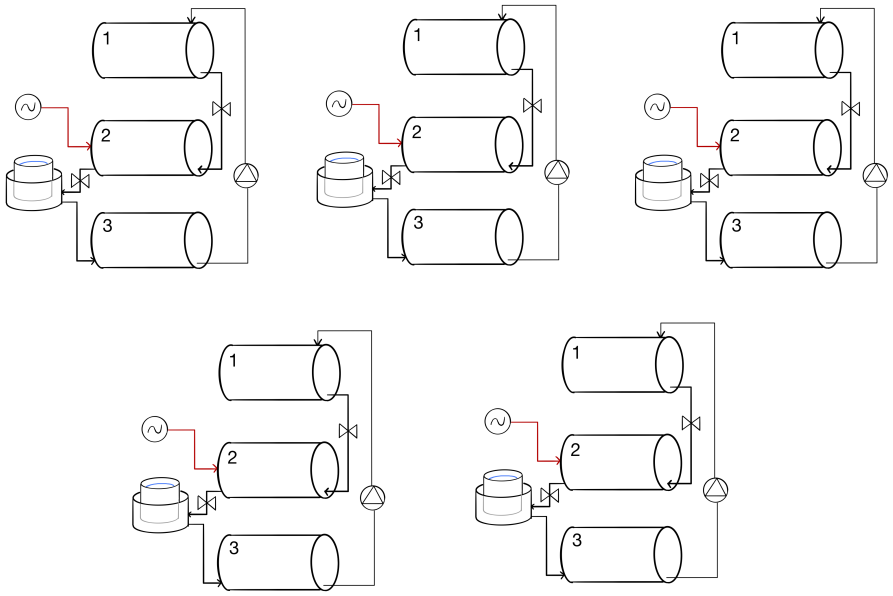

Figure 3.9: Possible configuration of cooking for 500 people. Five standalone systems are constructed to feed 100 people each.

A second configuration was featuring a new design was also proposed. The three tanks were sized so a single full storage tank could provide enough heat to cook 500 portions. The modification to the system is that the central storage tank connects to five separate cooking units, that each has the capacity to cook for 100 people, as seen in figure 3.10. The surface area and volume of tanks 1, 2 and 3 were thus changed and one fifth of $\hat{m}_{2P}$ flows into each cooking pan.

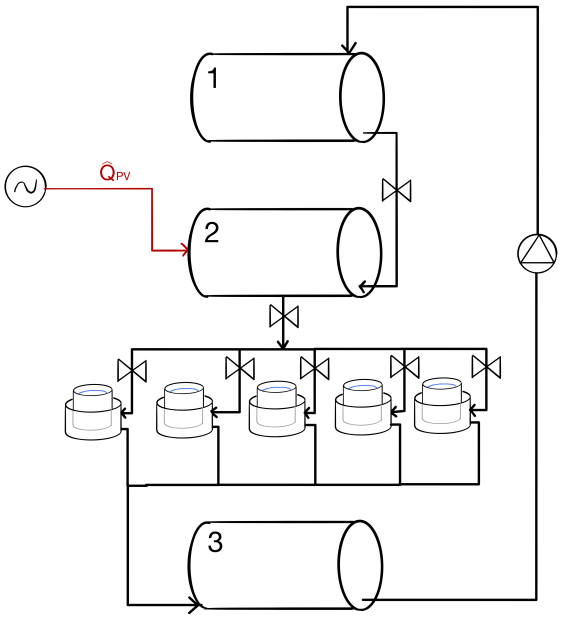

Figure 3.10: Second configuration of cooking for 500 people. The three oil tanks are increased in size, with oil from the central storage tank provided to five separate cooking units.

3.9.2 Additional PF Unit

A second alternative configuration was considered. The outlet of the cooking pan typically has a temperature of over 100 °C. In order to utilize more of this energy, the addition of a second water heating unit was modeled, as seen in figure 3.11. As before, the mass flow of $\hat{m}_{2P}$ was adjusted to control the temperature of control volume F. The oil flows through through a second cooking pan, heating a second casserole of water before accumulating in tank 3. The temperature of the second water control volume then depends on the mass flow $\hat{m}_{2P}$ as well.

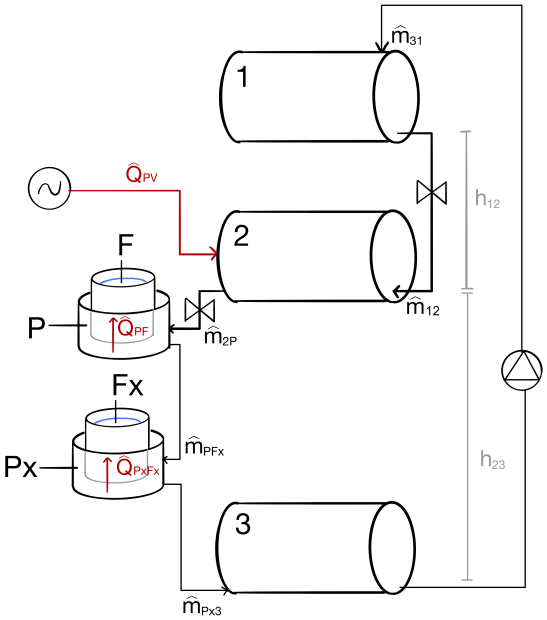

Figure 3.11: Alternative configuration to extract more energy from the outlet exiting the cooking pan. A second PF unit is added to heat more water.

3.9.3 Two Tank System

To possibly reduce heat losses, a third alternative configuration of the system was considered, where tank 3 is removed from the system. Instead of accumulating oil in the bottom tank, the oil is pumped directly from the outlet of the cooking pan back to tank 2, as seen below in figure 3.12. The pumping rate was determined by the temperature control of F. A second, manual pump is installed to pump from tank 2 to tank 1 when desired.

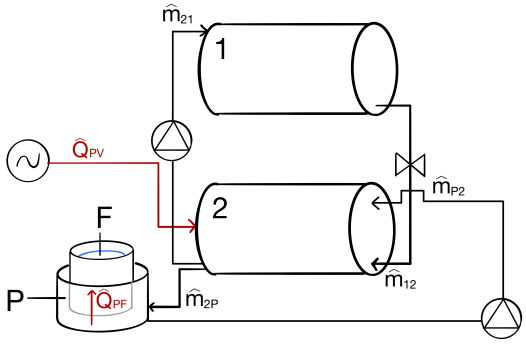

Figure 3.12: Alternative configuration to possible reduce heat losses from the system. The oil is pumped directly from the outlet of the cooking pan back to tank 2. A second pump is installed to pump from tank 2 to tank 1.

3.10 Maximum Available Solar Panel Effect $\hat{Q}_{PV,max}$

The output energy of the heating elements depends on the effect produced by the solar panels. During sunshine hours, the effect is larger than at cloudy conditions. Data from two field tests in Arusha of March 2019 performed by Thaule et.al. (2019) [8], were used to model the power generation at different weather conditions. The field tests used six solar panels with a rating of 304.1 W. An average effect per panel at various reported weather conditions from very cloudy to strong sun were calculated and are reported below in table 3.5. The recorded measurements from the field tests can be found in the appendix in tables D.1 and D.2.

Table 3.5: Modeled solar panel effects at different weather conditions.

Weather	Average effect per panel [W]
Strong sun	263.9
Sunny	213.2
Partly cloudy	163.1
Cloudy	121.1
Very cloudy	66.7

The number of solar panels available was increased from six during field tests to ten for

modeling. This was done as both field tests and initial simulations showed additional energy would be required to cook twice in a day. Figure 3.13 shows the modeled maximum available effect, $\hat{Q}_{PV,max}$, during sunny, mixed and cloudy weather conditions in case study 2, when varying weather performance was considered. Note that the effects are modeled to follow the general behavior of the field tests and are not a statistical representation of measurements from Arusha.

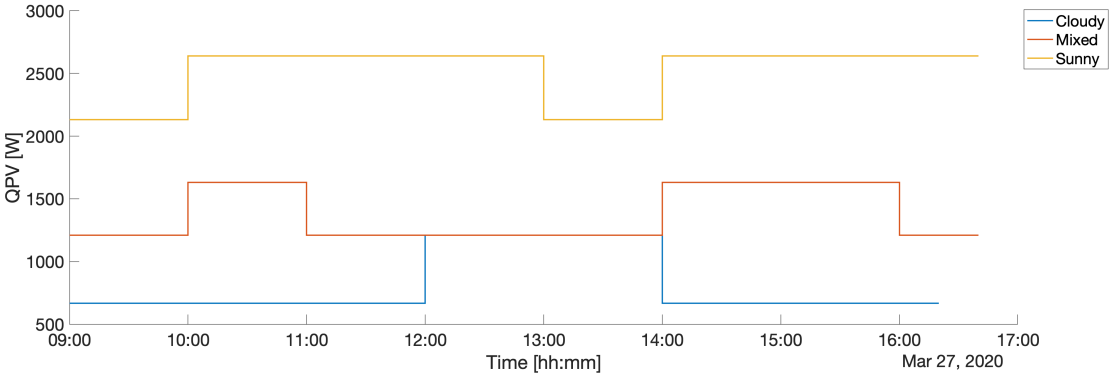

Figure 3.13: Plots of the modeled maximum available solar panel effect, $\hat{Q}_{PV,max}$, during different weather conditions.

3.11 Heat Transfer Coefficients

The key heat transfer coefficient in the system is the heat loss coefficient of tank 2, U_2. This is because tank 2 is insulated to store the energy from the solar panels and therefore directly affects the cooking capacity. The coefficient was experimentally determined where tank 2 was heated to 226 °C and the heating was shut off. The temperature was recorded every five seconds. The heat loss from the tank in the interval was calculated as

$$\hat{Q}_{2Ri} = m_2 Cp(T_{2i} - T_{2i-1})\frac{1}{dt} \tag{3.39}$$

where T_{2i} and T_{2i-1} are the current and previous temperature measurement of the system and dt the time interval between measurements.

Then, equation 3.28 was rearranged, using the average temperature of tank 2 in the time interval. Solving for the heat transfer coefficient, the following expression was obtained

$$U_{2i} = \frac{\hat{Q}_{2Ri}}{A_{tank}(\frac{T_{2i} + T_{2i-1}}{2} - T_{Ri})} \tag{3.40}$$

The average coefficient over a time interval was then calculated as

$$U_2 = \frac{\sum_{i=1}^{n} U_{2i}}{i} \tag{3.41}$$

The average coefficient was calculated over the first one, two, four, six twelve and 24 hours of the experiment. The average value of 2.1 W/m^2K was used. The data for each calculation is found in the appendix in table A.1. Tank 1 and 3 are not insulated and it was assumed the tanks' heat transfer coefficients were ten times larger than that of tank 2. The simple assumption was considered reasonable as the tanks have a main purpose of transporting and storing mass, making the exact temperature of less importance than in tank 2.

The overall heat transfer coefficient h_{PF} was calculated by considering that the heat flow must pass through the metal casserole, with a thickness dx and a conductivity k, before the casserole surface heats the water

$$h_{PF} = \frac{1}{\frac{dx}{k} + \frac{1}{h_w}} \tag{3.42}$$

where h_w is the convective heat transfer coefficient in the water. h_{PR} was assumed to be of equal value to h_{PF}. h_{PF} is a result of heat transport through metal and liquid, while h_{PR} is a result of transport from liquid to gas. As the oil is directly exposed to air for h_{PR}, there is no thermal resistance through metal. However, gases such as air generally have a lower heat transport than liquid, so these effects were assumed to even out. h_{FR} was assumed to be half as large. Being a result of transport through metal and gas, the heat transfer is expected to be lower than h_{PF}. These three heat transfer coefficients are important for the cooking capacity of the system. Due to their associated uncertainty, in particular for h_{FR} and h_{PR}, a sensitivity analysis was performed by calculating the first study of sizing the storage tank, described in more detail in chapter 4, with varying magnitudes of the three parameters.

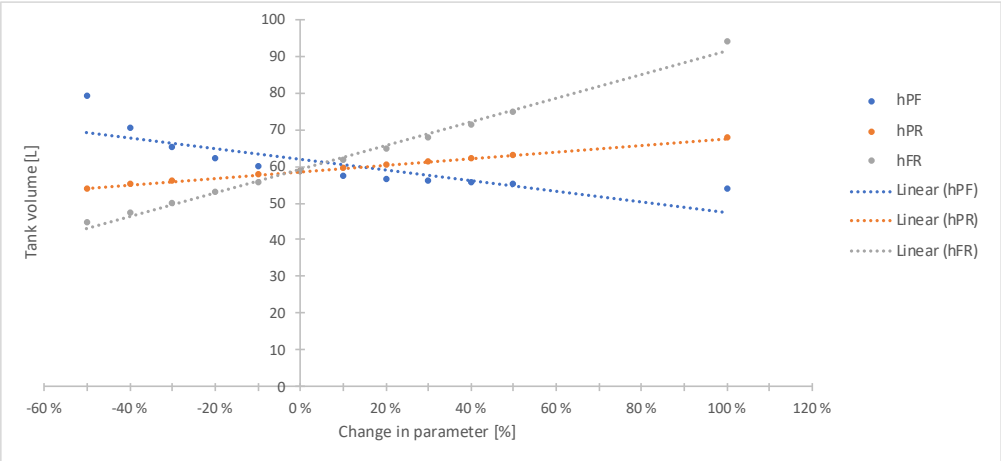

Figure 3.14: Sensitivity analysis of the heat transfer coefficients h_{PF}, h_{PR} and h_{FR} by calculating the minimum tank size with varying parameters.

As seen in figure 3.14, changing h_{PR} has the lowest effect on the required tank size. Only a small part of the surface oil in the cooking pan is exposed to air, resulting in a relatively small magnitude of heat transfer compared to $\hat{Q}_{PF}$ and $\hat{Q}_{FR}$. Both h_{PR} and h_{FR} show an almost linear relationship with the tank size. The heat loss from the surface of the casserole is modeled to have a big influence on the tank size, because the casserole is a quite large non-insulated surface. The study also indicates the importance of having good thermal conductivity through the casserole, illustrated by the variation of h_{PF}. If the conductivity is very low, much more oil is required to heat the oil. As the heat transfer coefficient becomes very large, the temperature difference of the cooking pan and water approaches zero. This occurs at an increase of 30 % of h_{PF}, where further increase of the parameter changes the resulting V_{tank} marginally.

3.12 Parameters

The constant parameters used in simulations are given below in table 3.6.

Table 3.6: Parameters used in MATLAB simulations.

Parameter	Description	Value Range	Unit	Reference
g	Acceleration of gravity	9.8	m/s^2	[18]
h_{12}	Pipe height difference tank 1 to 2	0.450	m	System
h_{23}	Pipe height difference tank 2 to 3	0.750	m	System
ρ	Density of oil	840	kg/m^3	[19]
Cp_{oil}	Heat capacity of oil	2242	J/kgK	[19]
Cp_{water}	Heat capacity water	4200	J/kgK	[18]
C_v	Manual valve discharge coefficient	0.5	-	System
d	Pipe diameter	0.015	m	System
a	Pipe area	1.767e-4	m^2	System
A_{v0}	Cross-sectional area of manual valve	1.963e-5	m^2	System
k	Steel thermal conductivity	16.3	W/mK	[20]
h_w	Average transfer coefficient in water	1500	W/m^2K	[21]
dx	Casserole bottom thickness	0.01	m	System
h_{PF}	Heat transfer coefficient casserole	781.15	W/m^2K	Estimate
h_{PR}	Heat transfer coefficient pan to room	781.15	W/m^2K	Estimate
h_{FR}	Heat transfer coefficient casserole to room	390.58	W/m^2K	Estimate
U	Heat transfer coefficient tank 1 and 3	21.0	W/m^2K	Estimate
U_2	Heat transfer coefficient tank 2	2.10	W/m^2K	Experimental
A_{PF}	Contact area pan and casserole	0.1838	m^2	System
A_{FR}	Heat transfer area casserole room	0.0990	m^2	System
A_{PR}	Heat transfer area oil and room	0.0141	m^2	System
T_R	Outside temperature	298	K	System

4 Case Studies

Tools

All simulations were performed in MATLAB R2017b on a Macbook Air 2013, using the CasADi framework to implement the optimization problems. CasADi is an open-source software tool for optimization and modeling, designed in particular for optimal control [22]. The optimal solutions were calculated using the NLP solver IPOPT and the direct multiple shooting algorithm.

Case Studies Structure

The simulations have been divided into several case studies to investigate the potential of the system. The titles of each study and the main problem to be answered are as follows:

1. Sizing of Storage Tank - how large should the tanks of the system be?
2. Weather Variation Effects - what is the cooking potential at varying PV panel electricity production?
3. Control Strategies during Cooking - how does the efficiency of current manual control during cooking compare to a more automated control?
4. Scale-up Designs and Their Energy Efficiencies - what is the best way of designing a larger system in terms of energy efficiency?
5. Scale-up Designs and Their Reliability - how likely is it that the large scale designs function over a longer period of time?
6. System Modification Study - how can the system be modified to utilize more of the stored energy?

4.1 Study 1: Sizing of Storage Tank

A central purpose of modeling the pilot system is to simulate the scale-up needed to provide food for a larger community. The cost of the system increases with the size of the tanks and amount of oil used. The design of the system was thus optimized to calculate the minimum minimum tank size required to cook using a full storage tank heated to the current design temperature of 513 K.

The following optimization problem of the system was established for sizing the storage tank

$$\min_{\hat{Q}_{PV}, D_{tank}, L_{tank}, \hat{m}_{2P}} \quad \psi := \frac{\pi}{4} {D_{tank}}^2 L_{tank} = V_{tank} \tag{4.1}$$

subject to the model reproduced in tables 3.2 and 3.3. The four control inputs are highlighted in green in figure 4.1.

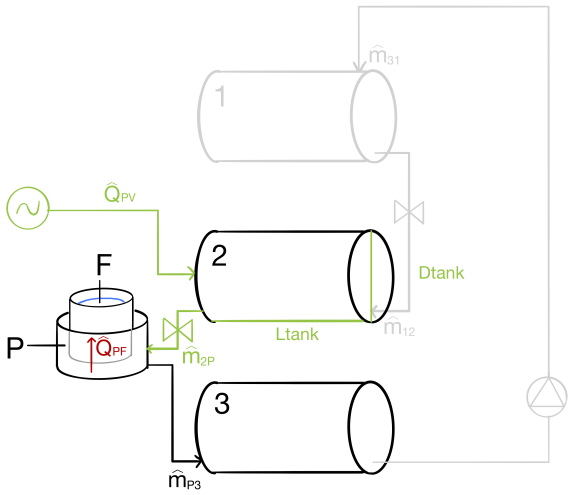

Figure 4.1: Illustration of the simulated cooking process. The four control inputs are illustrated in green. There is no additional filling from tank 1 to tank 2 during the process, and no circulation from tank 3 back to tank 1.

The water should be brought to boiling temperature in a reasonable time. Afterwards, the water must boil for an additional 20 minutes to cook the rice. The simulation was run with the requirement of heating the water very fast (within 5 minutes) to very slow (in 20 minutes), while varying the amount of water in the casserole, m_F. The mass flow through the cooking pan, $\hat{m}_{2P}$, was controlled directly like in equation 3.20b, and adjusted in control intervals of 5 minutes. Table 4.1 below shows the simulation times and the resulting number of control intervals, N, used in each series of simulations.

Table 4.1: Simulation times and number of control intervals.

Cooking strategy	Heating time [min]	Boiling time [min]	Total time [min]	N
Very fast	5	20	25	5
Fast	10	20	30	6
Slow	15	20	35	7
Very slow	20	20	40	8

As mentioned, tank 2 has been heated to 513 K, while the remaining control volumes are at room temperature. The initial mass of tank 2, $m_2(0)$, is not fixed as this depends on the tank size. To ensure that the tank is not emptied before cooking is completed, the tanks were sized to maintain at least 10 kg of oil after cooking at optimal control. The water mass, m_F, was fixed at values between 3 to 20 kg in each experiment.

During heating, the temperature of the water has not reached boiling, corresponding to the constraint of $T_{Fheating}$ between the ambient and boiling temperature. At boiling, the water must remain at a minimum of boiling temperature and was allowed to increase somewhat to loosen constraints and ensure convergence, denoted $T_{Fboiling}$. Thus, the following initial conditions of equation 4.2 and state constraints of equation 4.3 on each control interval were used

$$\begin{array}{cc} T_1(0) = 298 & [\text{K}] \\ T_2(0) = 513 & [\text{K}] \\ T_P(0) = 298 & [\text{K}] \\ T_F(0) = 298 & [\text{K}] \\ T_3(0) = 298 & [\text{K}] \\ m_1(0) = 1 & [\text{kg}] \\ 10 \leq m_2(0) \leq 300 & [\text{kg}] \\ m_P(0) = 0.5 & [\text{kg}] \\ 3 \leq m_F(0) \leq 20 & [\text{kg}] \\ m_3(0) = 1 & [\text{kg}] \end{array} \tag{4.2}$$

$$\begin{array}{cc} 298 \leq T_1 \leq 516 & [\text{K}] \\ 513 \leq T_2 \leq 516 & [\text{K}] \\ 373 \leq T_P \leq 516 & [\text{K}] \\ 298 \leq T_{Fheating} \leq 378 & [\text{K}] \\ 373 \leq T_{Fboiling} \leq 378 & [\text{K}] \\ 298 \leq T_3 \leq 516 & [\text{K}] \\ 1 \leq m_1 \leq 300 & [\text{kg}] \\ 10 \leq m_2 \leq 300 & [\text{kg}] \\ 0.5 \leq m_P \ \leq 1 & [\text{kg}] \\ 3 \leq m_F \ \leq 20 & [\text{kg}] \\ 1 \leq m_3 \leq 300 & [\text{kg}] \end{array} \tag{4.3}$$

For this problem, four control inputs were used, shown below in equation 4.4. The temperature of tank 2 is adjusted by limiting the solar panel input, $\hat{Q}_{PV}$. The temperature in the water depends on the mass flow $\hat{m}_{2P}$. Finally, the volume of the tank depends on D_{tank} and L_{tank}, which must be large enough to to contain the required mass flow.

$$
\begin{aligned}
0 \leq \hat{Q}_{PV} \leq 2639 \quad & [\text{W}] \\
0.3 \leq D_{tank} \leq 1.0 \quad & [\text{m}] \\
0.3 \leq L_{tank} \leq 0.7 \quad & [\text{m}] \\
0 \leq \hat{m}_{2P} \leq 1 \quad & [\text{kg/s}]
\end{aligned}
\tag{4.4}
$$

Additional constraints were added to ensure feasibility of the solution. The optimized tank diameter and length must remain constant in each control interval. In addition, inequality constraints were added so the volume of oil did not exceed the tank volume

$$
\begin{aligned}
D_{tank,i} &= D_{tank,1} \text{ for i} > 1 \\
L_{tank,i} &= L_{tank,1} \text{ for i} > 1 \\
V_{tank} &\geq \frac{m_2}{\rho} \\
V_{tank} &\geq \frac{m_3}{\rho}
\end{aligned}
\tag{4.5}
$$

A large scale system should have the capacity to cook 100 portions of rice with a full storage tank, without the need for additional filling or heating. This is approximately 4.5 kg dry rice, which requires 12 kg of water for cooking [23]. An average of the optimized tank sizes for 12 kg of waters were used in further simulations, excluding any significant outliers.

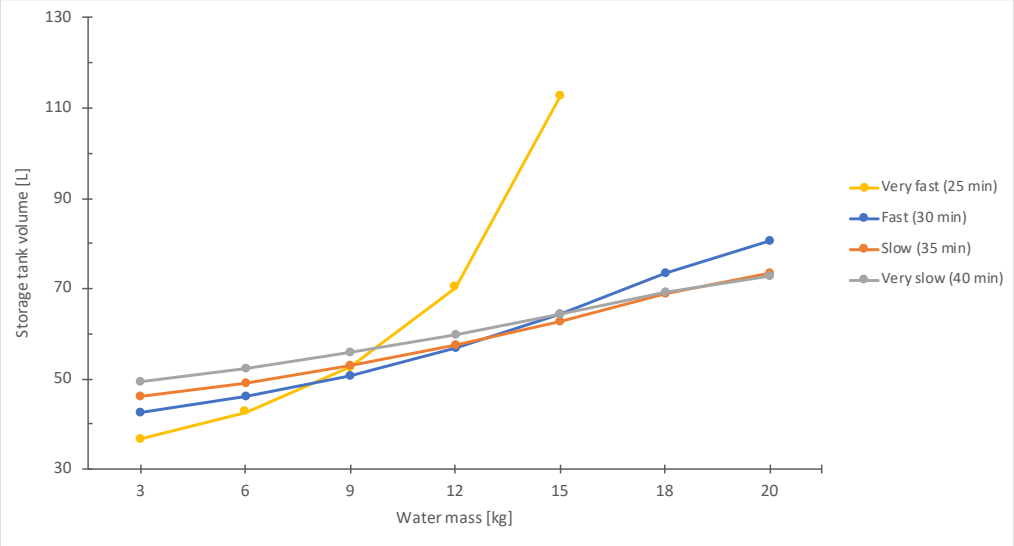

Figure 4.2: The tank size required when boiling temperature must be reached in 5 to 20 minutes, for a total cooking time of 25 to 40 minutes respectively.

The tank size varies depending on how quickly the water should reach 100 °C and the mass of water to be heated. The calculated recommended tank sizes are reported in figure 4.2. The average tank size of cooking in 30 to 40 minutes was 58 L, with $D_{tank} = 0.41$ m and $L_{tank} = 0.44$ m.

As seen in figure 4.2, the required tank volume is quite similar for low water contents in the casserole. As the water mass increases, it becomes challenging to heat the tank fast enough at short time intervals. The storage tank drastically increases in size, which is due to the fact that a large amount of oil mass must flow through the system to heat up the water quickly enough.

The optimized diameter and tank length are only sized to provide a sufficient tank volume. While the tank volume is thus optimal, other dimensions for the diameter and length might be optimal. For instance, a standard 60 L barrel could be purchased rather than a customized dimension to save cost. The calculated tank size of 58.5 L and 49.1 kg of oil is very similar to the current dimensions of the system in Arusha (60 L). This indicates that the current system has the potential of cooking for 100 people already. Field tests by Thaule et.al. (2019) from Arusha used 11 kg of hot oil to cook 1 kg of rice. Assuming a linear relation between oil consumption and amount of rice, this would require 49.5 kg oil to cook 4.5 kg rice (100 portions). This matches the model estimation of 38.1 kg oil needed quite well. The model match is even more promising when considering that the rice in the field

test rice was overcooked, with the authors pointing out that significantly less oil would have been necessary [8].

4.2 Study 2: Weather Variation Effects

In order to successfully use the system for cooking, sufficient amounts of energy must be stored. Thus, a study of varying weather conditions and resulting power supply was conducted. In all four optimization problems considered, the system was turned on at 09:00, using the following initial conditions

$$\begin{aligned}
T_1(0) &= 298 \quad [\text{K}] \\
T_2(0) &= 298 \quad [\text{K}] \\
T_P(0) &= 298 \quad [\text{K}] \\
T_F(0) &= 298 \quad [\text{K}] \\
T_3(0) &= 298 \quad [\text{K}] \\
m_1(0) &= 49.1 \quad [\text{kg}] \\
m_2(0) &= 1.0 \quad [\text{kg}] \\
m_P(0) &= 0.5 \quad [\text{kg}] \\
m_F(0) &= 12.0^{1} \quad [\text{kg}] \\
m_3(0) &= 1.0 \quad [\text{kg}]
\end{aligned} \tag{4.6}$$

4.2.1 Minimal Required Heating Input

The first part of this study solved an optimization problem to calculate the minimum constant power input the system needs to be heated in seven hours, ending at 16:00. This was done to scale the amount of solar panels required to heat the system twice during a day. The second control input, $\hat{m}_{12}$, was controlled every 20 minutes to gradually fill tank 2 at a temperature between 513 and 516 K. The objective function was then as shown in equation 4.7.

$$\underset{\hat{Q}_{PV},\hat{m}_{12}}{min} \quad \psi := \hat{Q}_{PV} \tag{4.7}$$

System state constraints were identical to that of equation 4.3, with two exceptions, as shown by equation 4.8. The mass of tanks 1, 2 and 3 were confined to the maximum sizing of 49.1 kg and the constraints on T_F are constant throughout the simulation as no cooking

[1] During cloudy weather, m_F is an optimization parameter.

was performed.

$$
\begin{aligned}
298 \leq T_1 \leq 516 \quad & [\mathrm{K}] \\
513 \leq T_2 \leq 516 \quad & [\mathrm{K}] \\
373 \leq T_P \leq 516 \quad & [\mathrm{K}] \\
298 \leq T_F \leq 378 \quad & [\mathrm{K}] \\
298 \leq T_3 \leq 516 \quad & [\mathrm{K}] \\
1 \leq m_1 \leq 49.1 \quad & [\mathrm{kg}] \\
1 \leq m_2 \leq 49.1 \quad & [\mathrm{kg}] \\
0.5 \leq m_P \leq 1 \quad & [\mathrm{kg}] \\
3 \leq m_F \leq 20 \quad & [\mathrm{kg}] \\
1 \leq m_3 \leq 49.1 \quad & [\mathrm{kg}]
\end{aligned}
\tag{4.8}
$$

The active control volumes and control inputs during heating of the storage tank are highlighted in figure 4.3.

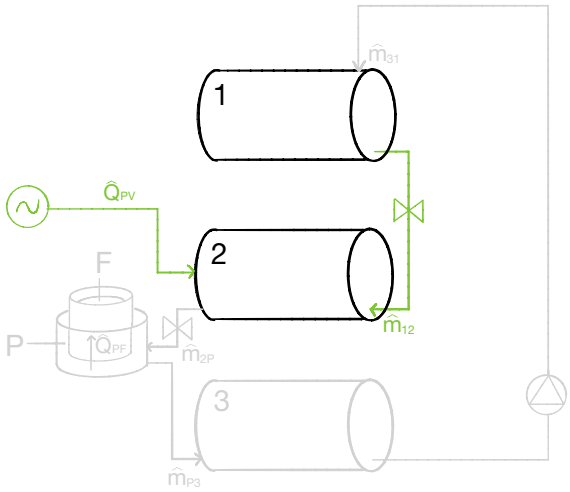

Figure 4.3: Illustration of the simulated heating process. The two control inputs are illustrated in green. Cold oil flows from tank 1 to tank 2 to limit the temperature in tank 2.

The following constraints on the inputs and control details were used, where t_N is the total simulation time

$$
\begin{aligned}
0 \leq \hat{Q}_{PV} \leq 2639 \quad & [\mathrm{W}] \\
0 \leq \hat{m}_{12} \leq 1 \quad & [\mathrm{kg/s}] \\
t_N = 7 \quad & [\mathrm{hours}] \\
\mathrm{N} = 21 \quad &
\end{aligned}
\tag{4.9}
$$

An additional constraint was added to the problem to maintain $\hat{Q}_{PV}$ constant in each control interval. The end states of tank 2 were also added as constraints, namely that T_2

reaches 513 K at the end of heating and that the tank must be full

$$\begin{aligned} \hat{Q}_{PV,i} &= \hat{Q}_{PV,1} \text{ for i} > 1 \\ T_2(end) &\geq 513 \quad [\text{K}] \\ m_2(end) &= 49.1 \quad [\text{kg}] \end{aligned} \tag{4.10}$$

Results and Discussion

Table 4.2 shows the minimum constant power input required to gradually fill up the tank completely at 513 K in 7 hours.

Table 4.2: Final parameters of heating with minimum constant solar input.

Parameter	Value	Unit
T_2(end)	513.0	K
m_2(end)	49.1	kg
$\hat{Q}_{PV}$	1310.4	W

Weather Effects

A successful system should be able to cook twice on a sunny day, namely for lunch and dinner. In order to cook two meals, it was assumed that the first heating should be done by 12:00. Further, a one hour window is allowed for cooking food and re-pumping the oil from the bottom tank to the upper tank by 13:00. At 16:00, the system should again be fully charged to cook once more. In establishing the case, three different scenarios were considered:

1. A sunny day - there is plenty of sun with high effect provided from the available solar panels. Cooking is possible for lunch at 12:00 and dinner at 16:00.
2. A day of mixed weather - periods of sunshine and clouds, with more moderate effect provided from the solar panels. Cooking is only possible for dinner at 16:00.
3. A cloudy day - mainly cloudy weather, resulting in significantly reduced effect of the solar panels. The stored energy is used to boil as much water as possible.

4.2.2 Weather Variations - A Sunny Day

During sunny weather, the cycle consists of five steps: heating, cooking for lunch, pumping of oil, re-heating and cooking for dinner. During heating, the objective was set to maximize the mass in tank 2 as early as possible, at a minimum temperature of 513 K. The state constraints were equal to that of the minimal power input study in equation 4.8. As with

the previous study, T_2 is controlled by the inflow of $\hat{m}_{12}$ and adjusting the effect of the maximum input of the heating elements, $\hat{Q}_{PV,max}$, illustrated previously in figure 3.13.

$$\max_{\hat{Q}_{PV},\hat{m}_{12}} \quad \psi := \int_0^t m_2(u)du \tag{4.11}$$

The following control details were used

$$\begin{array}{cc} 0 \leq \hat{Q}_{PV} \leq \hat{Q}_{PV,max} & [\text{W} \\ 0 \leq \hat{m}_{12} \leq 1 & [\text{kg/s}] \\ t_N = 3 & [\text{hours}] \\ \text{N} = 9 & \end{array} \tag{4.12}$$

During cooking, the objective was to minimize the amount of oil used from tank 2, as shown in equation 4.13, with constraints on the temperature of tank 2. The water must reach boiling within 20 minutes, and remain boiling for the final 20 minutes of the simulation.

$$\min_{\hat{Q}_{PV},\hat{m}_{2P}} \quad \psi := \int_0^t \hat{m}_{2P}(u)du \tag{4.13}$$

The system constraints were the same as in equation 4.3 for the sizing of the storage tank, but again with a maximum limit on m_1, m_2 and m_3 of 49.1 kg. The control details were as follows

$$\begin{array}{cc} 0 \leq \hat{Q}_{PV} \leq \hat{Q}_{PV,max} & [\text{W}] \\ 0 \leq \hat{m}_{2P} \leq 1 & [\text{kg/s}] \\ t_N = 40 & [\text{minutes}] \\ \text{N} = 8 & \end{array} \tag{4.14}$$

During pumping, the objective function followed that of equation 4.15, by maximizing the final amount of oil in tank 1, with only the pumping rate, $\hat{m}_{31}$, being an active mass flow.

$$\max_{\hat{Q}_{PV},\hat{m}_{31}} \quad \psi := m_1(end) \tag{4.15}$$

The state constraints equaled that of equation 4.8 and the following control details were used

$$
\begin{aligned}
0 \leq \hat{Q}_{PV} \leq \hat{Q}_{PV,max} \quad & [\mathrm{W}] \\
0 \leq \hat{m}_{31} \leq 1 \quad & [\mathrm{kg/s}] \\
t_N = 20 \quad & [\mathrm{minutes}] \\
\mathrm{N} = 4 &
\end{aligned}
\tag{4.16}
$$

Each of the five steps were simulated in separate scripts. The final states of each simulation were used as initial conditions in the next step.

Results and Discussion

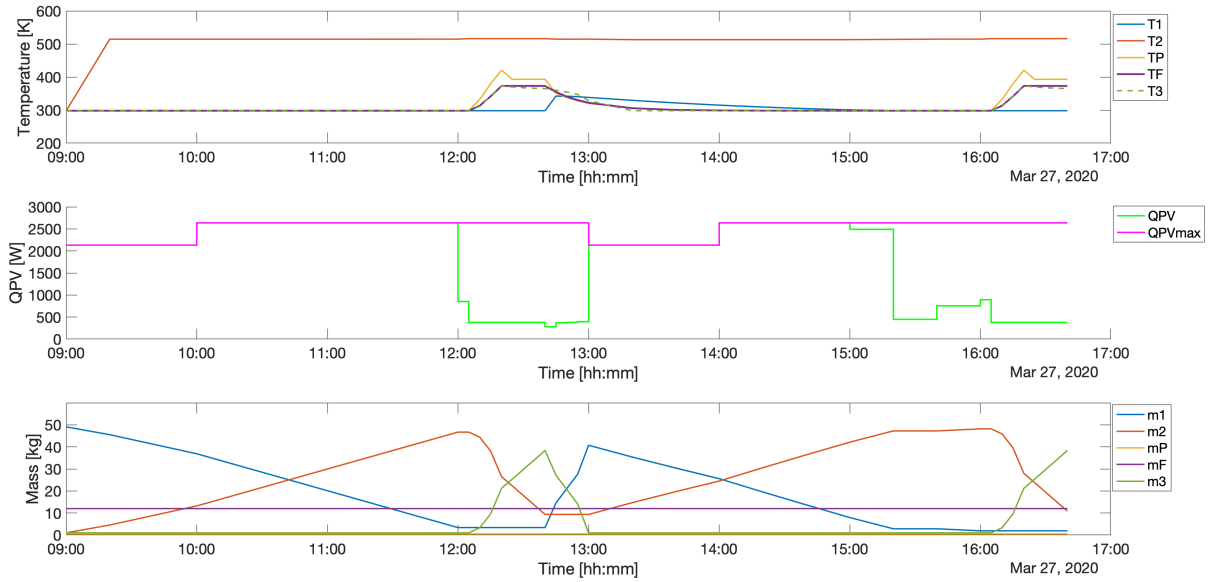

Figure 4.4: System states and solar input during a day of sunny weather. Top to bottom: 1. Temperatures in the control volumes 2. Solar power input available, $\hat{Q}_{PV,max}$ and used, $\hat{Q}_{PV}$. 3. Mass in the control volumes.

As seen in figure 4.4, cooking is performed from 12:00 - 12:40 and 16:00 - 16:40 as shown by the rise in temperature in the water, T_F. Pumping is done between 12:40 - 13:00, when the mass in tank 3, m_3 is emptied and tank 1 gradually fills up.

During sunny conditions, the system is able to cook twice a day, as shown in figure 4.4. The results also indicate that it is possible to cook with the system again at 15:20 when tank 2 is full, which is earlier than the proposed cooking at 16:00. It should also be observed that the available solar effect $\hat{Q}_{PV,max}$, exceeds the required input during cooking and from 15:00 - 16:40. No additional cooling can be achieved from $\hat{m}_{12}$ because m_1 is at is minimum of 1 kg. Therefore, the solar input is thus reduced to limit T_2 below 516 K, which means

that energy that could have been stored is wasted instead. One way of storing more of the energy would be to start pumping oil from tank 3 to tank 1 while cooking. Then, $\hat{m}_{12}$ could be initiated to fill tank 2 with colder oil from tank 1 while it is heated. The solution could be impractical as it requires someone to pump manually while the system is cooking.

4.2.3 Weather Variations - A Mixed Weather Day

During mixed weather, the power input is sufficient to heat the storage tank to 513 K within 7 hours in order to cook for dinner. The simulation thus followed the two first two steps of the sunny scenario, with heating followed by cooking. Thus, the optimization problems were identical to that of equations 4.11-4.14, except with a heating period of 7 hours with 21 control intervals.

Results and Discussion

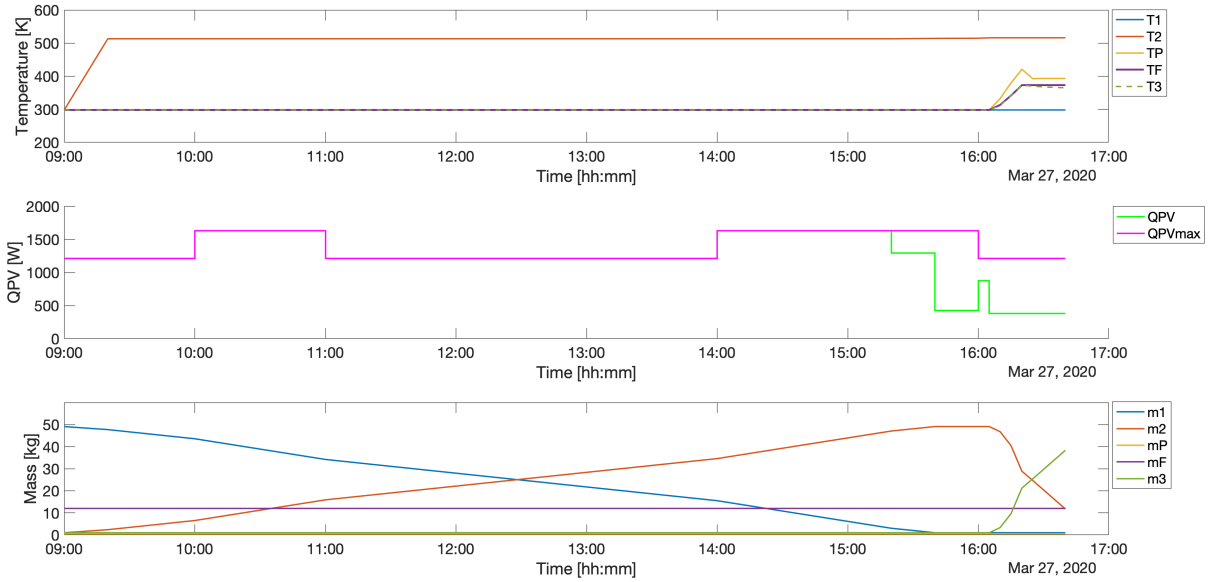

Figure 4.5: System states and solar input during a day of mixed weather. Top to bottom: 1. Temperatures in the control volumes 2. Solar power input available, $\hat{Q}_{PV,max}$ and used, $\hat{Q}_{PV}$. 3. Mass in the control volumes.

When the solar panel effect is lowered due to shifting cloudy and sunny weather, the system is specified to cook for dinner only, as shown in figure 4.5. This is illustrated by the rise of temperature in T_F starting at 16:00, and the decrease in m_2 while m_3 increases. Not all of the available effect is used to heat the system in seven hours, as seen in figure 4.5. Thus, the simulations indicate that cooking can be started earlier than 16:00, before tank 2 is completely filled. With the modeled weather, cooking can be initiated at 15:40 instead.

Alternatively, it also means that the available effect from the solar panels can be somewhat lower than modeled and still provide enough energy for cooking at 16:00.

4.2.4 Weather Variations - A Cloudy Day

The cloudy weather could limit the stored energy from boiling water for 20 minutes. However, it could still be of interest to heat water to boiling temperature for other applications such as making tea, washing hands or doing dishes. Therefore, the cloudy weather study consisted of heating the tank in 7 hours, followed by twenty minutes for heating the water to boiling temperature. This differs from the sunny and mixed weather case as the remaining 20 minutes of boiling was excluded.

Two strategies were considered for storing the energy. In the first scenario, tank 2 is filled while requiring a tank temperature of minimum 513 K. This is identical to the heating during the mixed weather scenario. Then, the amount of water that could be brought to boiling with this heated oil was calculated

$$\underset{\hat{Q}_{PV},\hat{m}_{2P}}{max} \quad \psi := m_F \tag{4.17}$$

The following control details were used

$$\begin{array}{cc} 0 \leq \hat{Q}_{PV} \leq \hat{Q}_{PV,max} & \text{[W]} \\ 0 \leq \hat{m}_{2P} \leq 1 & \text{[kg/s]} \\ t_N = 20 & \text{[minutes]} \\ \text{N} = 6 & \end{array} \tag{4.18}$$

In the second scenario, tank 2 was required to be completely filled in the seven hours, while maintaining as high of a temperature as possible

$$\underset{\hat{Q}_{PV},\hat{m}_{12}}{max} \quad \psi := T_2(end) \tag{4.19}$$

The system state constraints are identical to that of equation 4.8, with the exception of T_2 allowing to drop to 403 K. An additional constraint was added to the final mass of tank 2 to ensure it is completely filled

$$m_2(end) = 49.1 \quad \text{[kg]} \tag{4.20}$$

Then, the maximum mass of water that could be boiled in 20 minutes was calculated in the identical way of when maintaining a maximum temperature at cloudy conditions, using equations 4.17 - 4.18.

Results and Discussion

The two strategies considered during cloudy conditions are illustrated below in figure 4.6. The first strategy of filling the tank as much as possible while keeping the temperature at 513 K (maximum temperature), maintains a high T_2 with a slow filling to increase m_2. The second strategy of completely filling the tank during the seven hours (maximum level) fills the tank much faster, but T_2 is consistently lower. The full plots for all ten system states can be found in the appendix in figures B.1 and B.2.

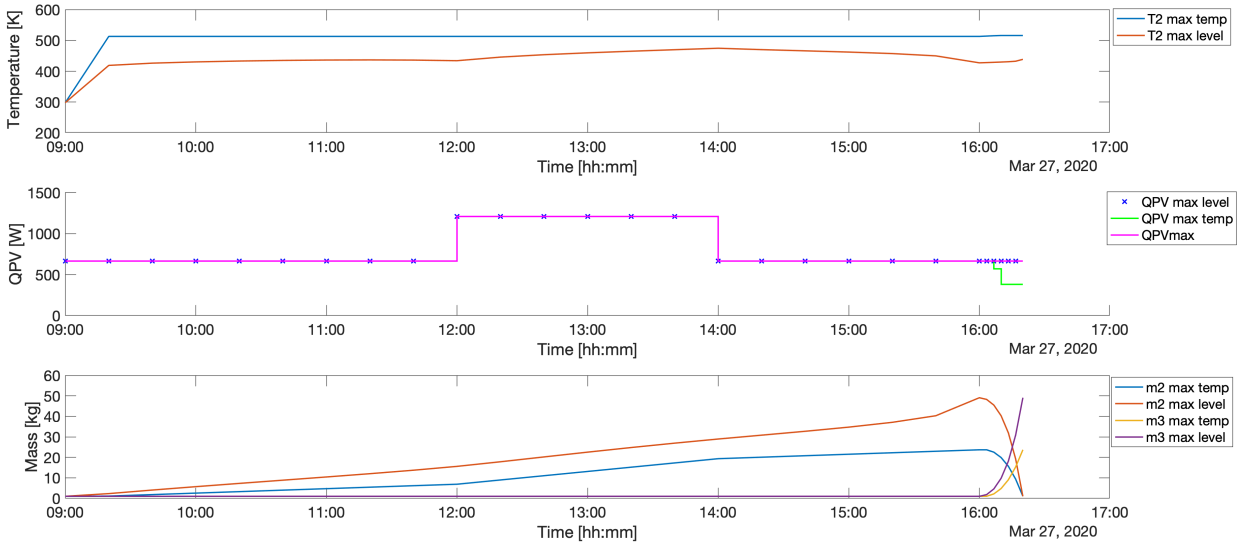

Figure 4.6: System states and solar input during a day of cloudy weather. Top to bottom: 1. Temperature in tank 2 2. Solar power input available, $\hat{Q}_{PV,max}$ and used, $\hat{Q}_{PV}$. 3. Mass in tank 2 and 3. The temperature is either kept constant at 513 K (max temp) or tank 2 is completely filled (max level) during heating.

As seen from figure 4.3, the modeled cloudy weather still provides enough heat to raise the water to boiling temperature. However, the energy is not sufficient to maintain water boiling for 20 minutes in either strategy. This can also be seen in light of figure 4.2. A minimum tank size of 40.4 L is required to heat 3 L of water. This corresponds to a consumption of 23.9 kg oil while maintaining 10 kg of oil in tank 2. This is slightly higher than the 23.7 kg of oil that can be heated to 513 K with the cloudy weather conditions.

Table 4.3 presents important system states pre-cooking at 16:00, and post-cooking at 16:40. Heating with maximum temperature could bring an m_F of 13.93 kg to boiling temperature.

Using the maximum level strategy could heat 9.13 kg water to boiling.

Table 4.3: Key system state values during the simulation of the two scenarios during cloudy weather

	Max Temperature	Max Level	Unit
T_2, pre-cooking	513.0	425.6	K
m_2, pre-cooking	23.69	49.10	kg
ΔH_{Tank2}, pre-cooking	11.42	14.04	MJ
T_F, post-cooking	373.0	373.0	K
m_F	13.93	9.13	kg
ΔH_{Food}, post-cooking	4.39	2.88	MJ
T_3, post-cooking	373.8	373.8	K
m_3, post-cooking	23.65	49.06	kg
ΔH_{Tank3}, post-cooking	4.02	8.34	MJ

It should be noted that the system is likely of little use during cloudy conditions. The main purpose of this system is to store excess energy when the production of electricity is high. It is therefore unlikely that the system will receive input energy on very cloudy days if the solar panels are connected to other utilities that have higher priority of usage.

Table 4.3 shows that more energy is stored in tank 2 when filling the tank completely, rather than maintaining a temperature of 513 K. This is because more energy is lost from the storage tank when the temperature is higher. However, maximizing the temperature is a more energy efficient process when the objective is to cook water. The total water mass boiled is much higher, at 13.93 kg versus 9.13 kg when maximizing the level. The significantly lower temperature achieved when filling tank 2 requires a high flow of oil through the pan. As a result, a lot of oil at a high temperature ends up in tank 3, which is considered "wasted energy" unless it is recycled through the system. For practical purposes, the water mass should be decreased somewhat unless optimal operation can be ensured, as there is a risk of running out of oil as an m_2 of only 1.0 kg remains after heating the water.

4.3 Study 3: Control Strategies During Cooking

In the previous study, the mass flow was optimized every five minutes during cooking with 8 control intervals over 40 minutes. It was therefore investigated whether there was a large difference in performance if the mass flow was optimized less or more frequently when cooking. As mentioned before, the current physical system relies on manual operation of a valve to adjust the flow $\hat{m}_{2P}$. If the valve opening is kept constant as tank 2 empties, the liquid level decreases, which decreases pressure difference and thus the mass flow. Therefore, it was also investigated how controlling the valve opening rather than the mass flow directly affects performance. The following control strategies were compared:

1. Simple automatic control - infrequent control of the mass flow directly (N = 6)
2. Careful automatic control - frequent control of the mass flow directly (N = 40)
3. Simple manual control - infrequent manual adjustment of the valve opening (N = 6)
4. Careful manual control - frequent manual adjustment of the valve opening (N = 40)

Weather conditions equaled that of cooking during sunny weather. The automatic control simulations are simply repetitions of the sunny cooking described in equations 4.13-4.14, with an altered amount of control intervals, N. For manual control, the physical valve opening was optimized, which in turn affects the mass flow. As seen in equation 4.21 below, the opening u_5 was the manipulated variable, rather than $\hat{m}_{2P}$ directly

$$\min_{\hat{Q}_{PV}, u_5} \quad \psi := \int_0^T \hat{m}_{2P} \tag{4.21}$$

where the mass flow equation derived in chapter 3 is repeated below

$$\hat{m}_{2P} = \rho \sqrt{\frac{2g(h_2 - h_3 + h_{23})}{\frac{1}{(C_v u_5 A_{v0})^2}}} \tag{4.22}$$

Results and Discussion

The optimal control inputs and the responses in temperature in the cooking pan and water are presented in figure 4.7.

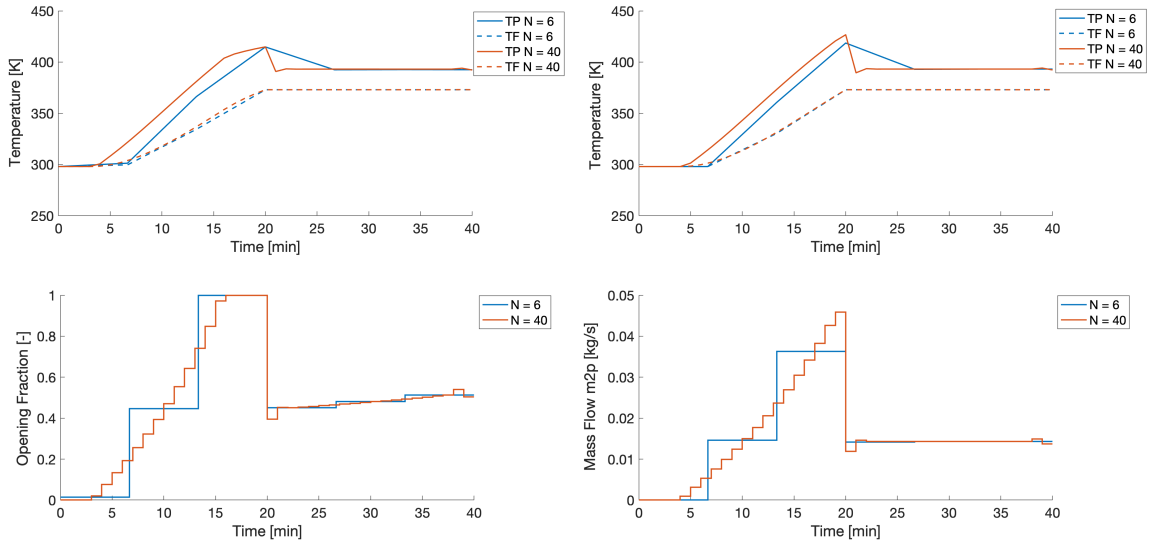

Figure 4.7: Left: Control profiles and temperature responses when controlling the opening fraction of the valve (manual control) at a low and high number of control intervals. Right: Control profiles and temperature responses when controlling the mass flow directly (automatic control) with a low and high number of control intervals.

In table 4.4 below, the mass and energy contents of tanks 2 and 3 are shown for the different cooking methods.

Table 4.4: Final masses, temperatures and enthalpies in tanks 2 and 3 after cooking by controlling the mass flow automatically or using a manual valve.

Strategy	m_2(end) [kg]	m_3(end) [kg]	ΔH_{tank2}(end) [MJ]	ΔH_{tank3}(end) [MJ]
Automatic control, N = 6	9.62	38.42	4.64	5.79
Automatic control, N = 40	9.97	38.07	4.80	5.74
Simple manual control, N = 6	9.46	38.58	4.56	5.74
Frequent manual control N = 40	9.74	38.25	4.69	5.64

Figure 4.7 indicates that a constant flow is required when the water has reached boiling. This is a consequence of the assumption that the outdoor temperature is constant. The frequent control profile gradually increases the mass flow to use as little mass as possible. However, table 4.4 shows that the strategy is probably more detailed than necessary, as $m_2(end)$ is very similar for six and 40 control intervals. The difference is also small between the manual and automatic control. This means that if operated optimally, the addition of a thermostatic valve therefore provides little advantage over the manual control.

Table 4.5 shows the energy efficiencies of the strategies for water heating. $\int_{t=0}^{t=boiling} \hat{Q}_{PV}$ notes the energy input from the solar panels from the start of heating tank 2 until the water

is boiling. A theoretical energy input of 3.78 MJ is required to boil the 12 kg of water, while the storage tank absorbs 27.45 to 27.66 MJ until the water is boiled.

Table 4.5: Energy efficiencies of the water heating

Strategy	$\int_{t=0}^{t=boiling} \hat{Q}_{PV}$ [MJ]	Theoretical need [MJ]
Automatic, N = 6	27.45	3.78
Automatic, N = 40	27.45	3.78
Simple manual, N = 6	27.66	3.78
Careful manual, N = 40	27.45	3.78

As seen in table 4.5, the enthalpy input to the system is very large compared to the energy stored in water. If the system is considered strictly as a water boiler, one could be tempted to call the efficiency were low. However, the results are promising when considering the system as a "dump load" for excess electricity that might otherwise be wasted. Additionally, a considerable amount of energy may be stored in the insulated storage tank for a later cooking process the same day or over night.

4.3.1 Further Analysis of Simple Manual Control

The simple manual control scenario was further analyzed by adjusting the precise optimal opening fractions to practically feasible valve opening strategies. The simulation was repeated by enforcing the practical valve openings and the difference in performance was analyzed.

It is likely that manual operation could deviate from the optimum, which reduces energy efficiency. To observe this effect, a second simulation series was performed with an exaggerated opening fraction of 0.05 to 0.15 above the practical strategy. For example, a strategic fraction of 0.5 was replaced by 0.55 for a deviation of 0.05. An opening fraction strategy of 1.0 was kept constant.

Results and Discussion

Below in table 4.6, the optimal opening fractions for simple control are reported. The recommended practically feasible opening fractions are also given.

Table 4.6: Optimized valve openings and practical valve opening strategy.

Time [s]	Optimal opening fraction [-]	Practical opening fraction [-]
0-400	0.0149	0.0
400-800	0.4457	0.5
800-1200	1.0000	1.0
1200-1600	0.4504	0.5
1600-2000	0.4811	0.5
2000-2400	0.5126	0.5

Applying the practical valve openings in the simulation results in a higher consumption of hot oil than the optimum, as shown in table 4.7.

Table 4.7: Final storage tank mass in the optimal and practically feasible scenario

Scenario	m_2(end) [kg]
Optimal simple manual control	9.46
Practical simple manual control	8.43

The effect of keeping the valve consistently more open than the practical optimum, from 0.05 to 0.15 are seen in figure 4.8 below. With the recommended practical openings, the remaining mass in the storage tank is 8.43 kg. The remaining mass is reduced to 0.95 kg when a consistently excessive opening fraction of 0.15 is applied.

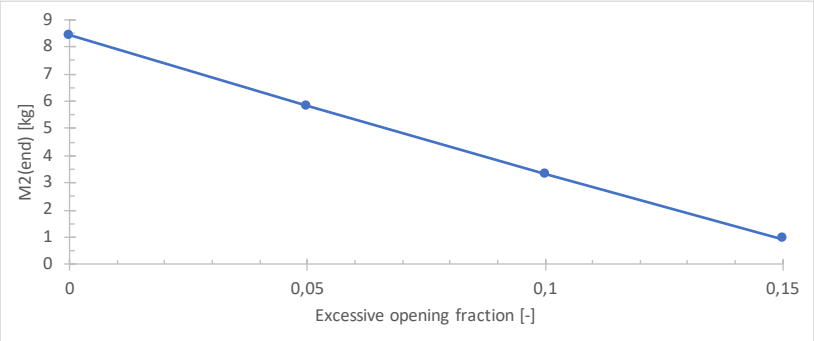

Figure 4.8: Remaining mass in tank 2, m_2(end) after cooking with consistently excessive opening fraction from the practical optimum.

As seen in table 4.6, the manual control strategy close to the optimal control is very simple, leaving the user to limit the flow between half and fully open. This is a very user-friendly strategy. The issue with the control strategy is that the valve positioning is hard to visually observe. As the system is now, it is hard to know how open the manual valve is, from the author's own experience with the physical system. It is also seen that the model is quite sensitive to excessive flow in figure 4.8. If the valve is consistently opened at an opening fraction 0.15 higher than the manual guideline, the storage tank is close to empty after

cooking. Another, possibly simpler cooking strategy could be implemented for the boiling in the final 20 minutes. As seen in figure 4.7, the optimized mass flow is near constant, with T_P maintained at 391 K. By installing a thermostat in the cooking pan, the response in temperature can be observed by the user while adjusting the valve.

Only energy efficiencies in terms of consistently too open valve was considered. It is probable that some users of the system will leave the valve too open, then adjust the flow too small before readjusting. This is also a less efficient method, but the significant end result will be the same: too much flow is used to reach the optimal cooking or the food is not fully cooked because the tank runs out of oil.

4.4 Study 4: Scale-up Designs and Their Energy Efficiencies

The system had so far been optimized to cook for 100 people. In order to cook for an even larger crowd, the system must either be scaled up or several smaller systems must be used. In the scale-up, a scenario of cooking for 500 people was considered, and the amount of energy that was absorbed in the different systems was calculated. In the first option, the use of five small systems were considered, as introduced in figure 3.9. The energy absorbed in one system was found by integrating the $\hat{Q}_{PV}$ inputs during the first heating of the sunny and mixed weather scenarios of case study 2. The total absorbed energy of the configuration was obtained by multiplying the energy by five.

In the second option, a modified single system consisting of larger oil tanks and five cooking units was modeled. This system was introduced in figure 3.10. The sizing of the system was performed by repeating study 1 with four additional sets of control volumes P and F. The resulting dimensions were used for the tanks and the sunny and mixed scenario of study 2 repeated with the new dimensions. As above, the integrated $\hat{Q}_{PV}$ was used to calculate the energy absorbed by the large system.

Results and Discussion

Table 4.8 below shows the required calculated dimensions of cooking for 500 people using the two configurations.

Table 4.8: System dimensions for the scale-up configurations of using five small units or one large. Unit values refer to dimensions of each individual system while total values are the sum of dimensions.

Configuration	Unit V_{tank} [L]	V_{tank} total [L]	Unit A_{tank2} [m^2]	A_{tank2} total [m^2]
Five small units	58.45	292.27	0.83	4.17
Single large unit	292.27	292.27	2.67	2.67

Table 4.9 reports the required heating input to cook for 500 people in the two system configurations. The two weather scenarios considered are a sunny day where heating is completed in three hours and a mixed weather day that completes heating in seven hours.

Table 4.9: Required heating input to fill the tank during a day of sunny weather (three hour heating) or mixed weather (seven hour heating).

Configuration	Sunny Weather [MJ]	Mixed Weather [MJ]
Five small systems	133.38	168.13
Single large system	131.50	149.59

The two configurations considered to cook for 500 people are calculated to require the same total tank size, as shown in table 4.8. The simulations indicate that less heating input is required to fill a centralized large storage tank compared to five smaller storage tanks. This follows from the modeled heat loss of tank 2 being directly proportional with the surface area of the tank. As seen in table 4.8, five smaller tanks have a higher total surface area at 4.17 m^2 compared to 2.67 m^2 for the single large tank. At a rapid heating time of three hours, the heat loss difference is quite small, as seen in table 4.9. When the heating is done in seven hours, the difference becomes much larger. Ultimately, the performance must also be considered in light of costs and practicality of the two designs, which is out of scope for this project.

4.5 Study 5: Scale-up Designs and Their Reliability

The reliability of the two configurations were also considered by calculating the probability that the configurations can operate for a period of two or five years without maintenance. Breakdown of the heating elements were considered as the only failure mode, using a generic failure rate of $\lambda = 5.57$ per 10^6 hours for electrical heaters, retrieved from literature [24]. The heating elements were assumed to have a exponential failure distribution, with the reliability of each component, $r(t)$, calculated as shown in equation 2.6. The calculation is shown in equation 4.23 for the reliability of one heating element after a period of two years.

$$r(t = 17520) = e^{-5.57 \cdot 10^{-6} \cdot 17520} = 0.907 \tag{4.23}$$

For the small systems, it was assumed that three heating elements were installed. All three elements had to work in a system for the system to be considered fully functional, with a reliability of the small system, $R_s(t)$, as shown in equation 4.24. The equation also includes a sample calculation for the two year period.

$$\begin{aligned} R_s(t) &= r(t)^3 \\ R_s(17520) &= 0.907^3 = 0.746 \end{aligned} \tag{4.24}$$

Then, the probability that one to five of the systems were functioning after two and five years was calculated, using equation 2.7. The calculation is exemplified in equation 4.25 for the probability that at least four out of five small systems function after two years.

$$R_s(17520) = \binom{5}{4} 0.746^4 (1 - 0.746)^{5-4} + \binom{5}{5} 0.746^5 (1 - 0.746)^{5-5} = 0.625 \tag{4.25}$$

For the single unit large system, four scenarios were considered. Either, the system is directly scaled up, using 15 heating elements to provide sufficient heating. All 15 must work for the system to be fully functioning, exemplified in equation 4.26 for a two year period. To reduce the chance of failure, a second scenario considered using 8 elements at twice the watt rating, assuming the same failure rate applied.

$$\begin{aligned} R_s(t) &= r(t)^{15} \\ R_s(17520) &= 0.907^{15} = 0.231 \end{aligned} \tag{4.26}$$

Finally, an extra heating element was introduced in each scenario, resulting in a k-out-of-n structure. Here, 15oo16 and 8oo9 structures were considered, meaning 15 out of 16 elements and 8 out of 9 elements were required to operate to fully function, respectively. The calculation is exemplified for the 15oo16 structure after a two year period in equation 4.27.

$$R_s(17520) = \binom{16}{15} 0.907^{15} (1 - 0.907)^{16-15} + \binom{16}{16} 0.907^{16} (1 - 0.907)^{16-16} = 0.554 \tag{4.27}$$

Results and Discussion

Figure 4.9 shows the reliability of using five separate systems. The plot illustrates the probability that a minimum amount of the five systems are functioning after two and five years.

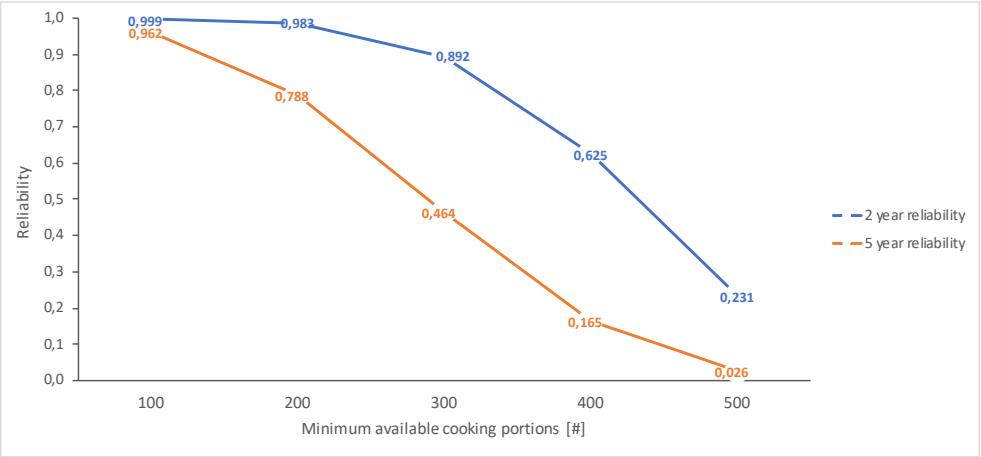

Figure 4.9: Reliability of the five small units configuration to cook a minimum amount of rice portions after a given period of time.

It is highly likely that at least one of the five small systems is working after a period of both 2 and 5 years, as seen in figure 4.9. However, maintenance has to be expected on at least one of the systems after two years, with a probability of 23.1 % for all five systems to be working. This is equal to the probability that the large system is working properly after two years, as both scenarios require all 15 heating elements to function. The benefit of several small systems is that it allows for maintenance on one system, while the others are operating.

In figure 4.10, the system reliability is plotted for a maintenance interval of two and five years, using a single system with a large centralized tank. The plot includes the four different heating element configurations discussed and the resulting probability that the system functions after the given period. The figure shows the benefit of reducing the amount of heating elements or introducing redundancy in the system. It is particularly interesting for the two year period, where going from a 15oo15 to a 15oo6 setup changes the probability from quite unlikely (23.1%) to more likely than not (55.4%) for the system to function. The effect is even more pronounced for the 8oo8 and 8oo9 scenario, where the probability is changed from less likely (45.8%) to quite likely (79.9%) function.

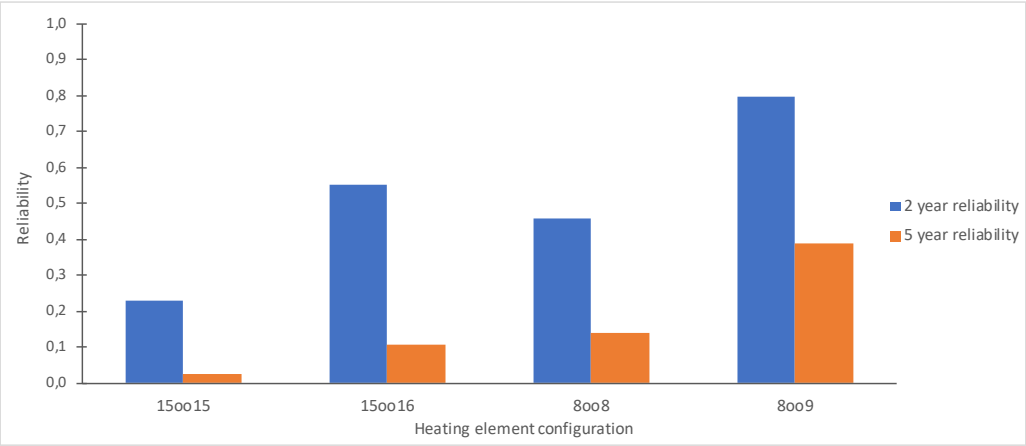

Figure 4.10: Reliability of the large system after two and five years, using a configuration of 8 to 16 heating elements. 8oo9 describes a redundancy where only 8 out of 9 elements are required for the system to function at maximum capacity. Equivalently, 15oo16 describes the use of 16 elements where 15 are required to function.

4.6 Study 6: System Modification Study

Both experimental tests and the simulations show that a significant amount of the mass that accumulates in tank 3 has a high temperature when exiting the cooker. Two alternative designs were therefore designed to utilize the energy more efficiently.

4.6.1 Additional PF Unit

The first design was introduced in figure 3.11, by adding a second cooking pan and casserole below the first one. The optimization problem followed that of the sunny cooking scenario with equations 4.13 - 4.14. The only difference was that $\hat{m}_{2P}$ flows through the second cooking pan before accumulating in tank 3. The intentions were to investigate the additional energy that could be stored in water.

Results and Discussion

The temperature profiles of the cooking pans and casseroles of water are shown below in figure 4.11. The temperature of the second water control volume, Fx, is maintained at 58 °C (331 K). A plot of all system states can be found in the appendix in figure B.3.

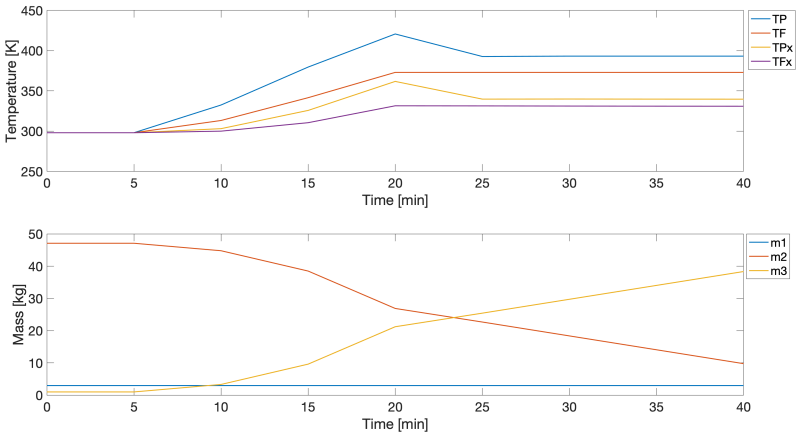

Figure 4.11: Mass and temperature profiles of the modified system with two water heating units during cooking on a sunny day.

In table 4.10 below, the total energy stored in water after cooking is shown for the original system and the modified design.

Table 4.10: Thermal energy stored in water in the original system and when the additional PF unit is added.

Configuration	PF Units	T_F(end) [K]	$T_{Fx}(end)$ [K]	Energy Stored [MJ]
Original system	1	373.00	-	3.78
Additional PF	2	373.00	330.92	5.44

The implementation of an additional water heating unit like the setup in figure 3.11, increases the amount of energy saved. This could be useful if the warm water can be used for other purposes or if another cooking batch is performed shortly after. Otherwise, the configuration is likely not very useful as it could be hard to maintain the temperature for a long time unless the casserole is highly insulated.

4.6.2 Two Tank System with Storage Recycle

The second design, introduced in figure 3.12, recycles the oil directly back to tank 2 after the cooking pan. The design was considered to have two possible benefits: reduce the heated mass required in tank 2 before starting cooking and reduce the time required to cook a second time during a day. The minimum required mass in tank 2 to cook during different weather conditions was calculated with the following optimization problem, with the control details of sunny cooking, described in equation 4.14.

$$\min_{\hat{Q}_{PV}, \hat{m}_{2P}} \quad \psi := m_2(0) \tag{4.28}$$

The problem was calculated for both the original three tank system and the modified two tank system and compared. The resulting minimum initial masses were recorded and plotted.

It was observed that the constrained pumping rate $\hat{m}_{2P}$ of 1.0 kg/s was reached in the final control interval for the two tank system. This pumping rate was considered quite high, so the very sunny conditions were repeated with a decreased maximum rate of 0.5 and 0.3 kg/s to investigate whether this produced significantly different results.

Finally, the time required to cook a second time for the two tank system was studied by running the full sunny day scenario of study 2, using the modified model equations for the two tank system.

Results and Discussion

Figure 4.12 shows the minimum amount of oil required in tank 2 at 513 K in order to cook at different weather conditions. The total $\hat{Q}_{PV}$ corresponds to the output of ten panels at very cloudy to strong sun, as described in table 3.5. Plots of the mass and temperature of tank 2 during the cooking is found in the appendix in figure B.4.

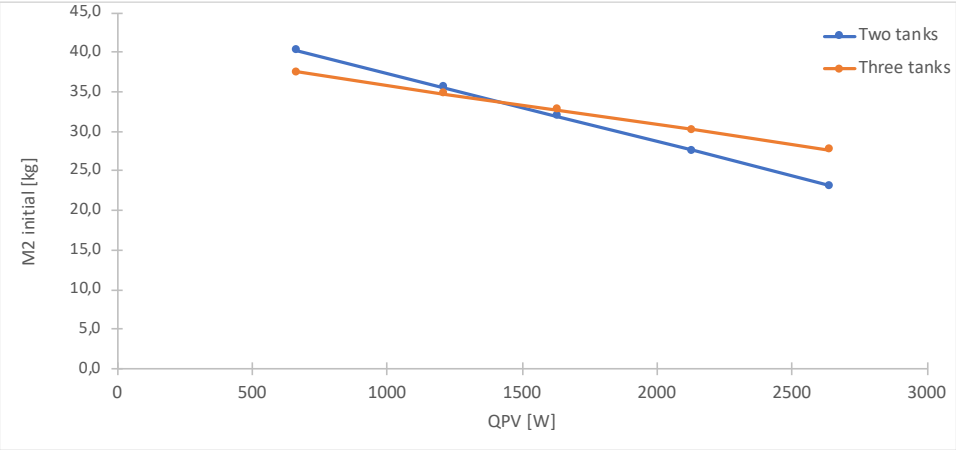

Figure 4.12: Minimal starting mass required in tank 2 when cooking with different solar panel inputs.

From figure 4.12, it is observed that the weather conditions during cooking greatly affects the system's cooking capability. If there is strong sun during the 40 minutes spent on cooking, the system only needs 23.1 kg pre-heated oil to cook 100 portions. On the other

hand, if the weather conditions are very cloudy, little additional heat is added to the storage tank, and a pre-heated amount of 40.2 kg oil is required. A possible way of increasing the predictability of the system is to actively monitor weather forecasts. If the next day is supposed to be sunny, the operators know that the system can be used both for lunch and dinner. If the next day is more cloudy, the operator knows that the system must be charged throughout the day to a minimum level of 40.2 kg oil before cooking at dinner time.

As shown in figure 4.13, the maximum capacity of the automatic pump for $\hat{m}_{2P}$ has little effect on the resulting performance. In all three cases, the required pumping rate is much lower than the constrained maximum except for in the final control interval. This indicates that a potential two tank system only needs a small pump to circulate oil back to the storage tank.

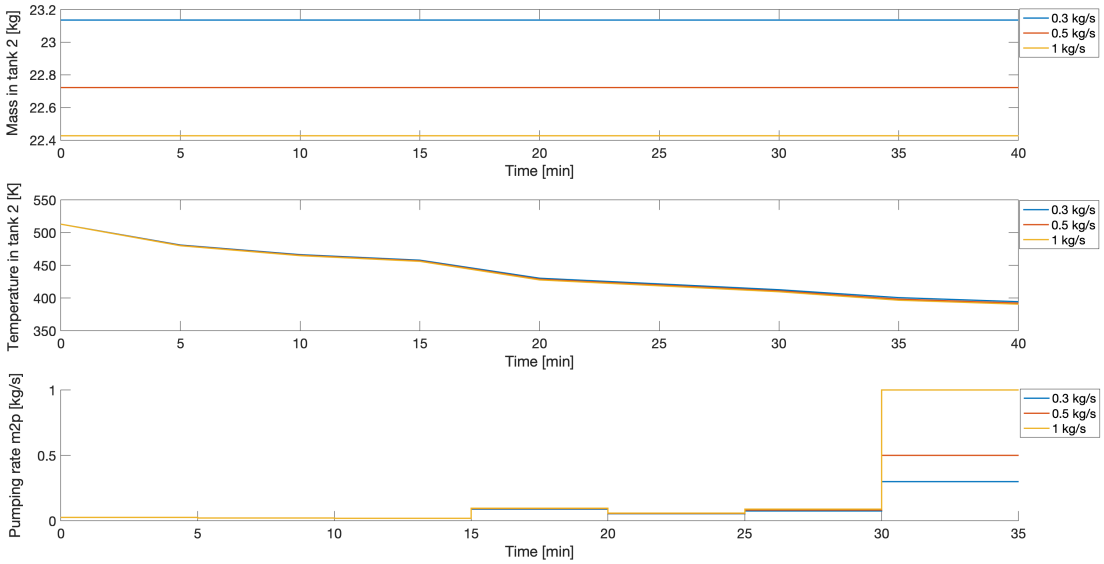

Figure 4.13: Minimal starting mass required in tank 2 during very sunny weather with different maximum pumping rates.

The results of running the sunny weather case with the two tank system are shown in figure 4.14. As seen from the plot of T_2, the system is full and heated to 513 K by 13:40, which is much faster than the three tank system that is fully charged at 15:20. Modifying the configuration to a two tank system thus saves a considerable amount of energy. It should be noted that there are some limitations to the results. The model assumes no heat losses from the pipes, which favors the direct recycle to tank 2 rather than heat losses associated with transporting the oil through tank 3 and tank 1 before returning to tank 2. In addition, the automatic pump transporting $\hat{m}_{2P}$ must be powered by the solar panels, which will drain some power that could otherwise have been used for heating tank 2.

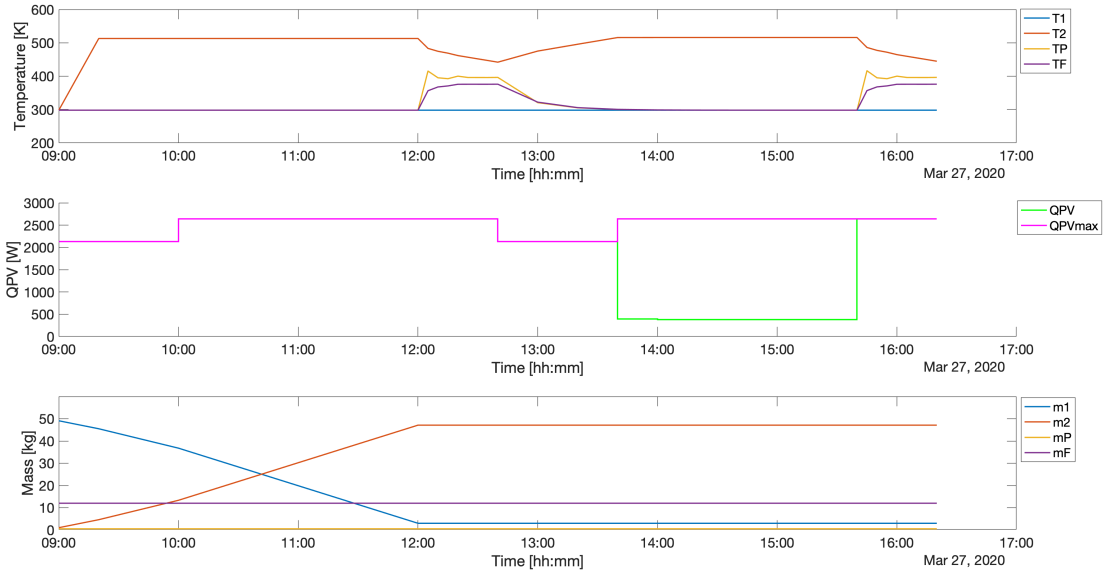

Figure 4.14: System states of the two tank system and solar input during a day of sunny weather. Top to bottom: 1. Temperatures in the control volumes 2. Solar power input available, $\hat{Q}_{PV,max}$ and used, $\hat{Q}_{PV}$. 3. Mass in the control volumes.

5 Discussion

5.1 Modeling Assumptions

Four modeling assumptions were identified as having a significant effect on the calculated cooking capacity: negligible heat loss from pipes, constant heat capacity and density of the oil and that all mass in the tank can be transported. Thaule et.al. (2019) report that the insulation of the pipes of the physical system works properly [8]. This indicates that the heat losses from the pipes are small and thus do not affect the cooking capacity to a large extent. The assumption of constant oil density overestimates the mass that can be stored in the tank at a high temperature and thus the cooking capacity. However, the heat capacity of the oil is also larger at higher temperatures, so more thermal energy can be extracted per kg oil before the temperature reduces. Therefore, these effects even each other out to some extent. Finally, the cylindrical shape of the tank will likely result in residual oil in the bottom of a tank that is not transported. As a safety measure, the tanks were sized by constraining a final of mass of 10 kg in tank 2 to ensure the tank would not run out of oil.

The modeling of $\hat{Q}_{PV,max}$ was based on data from field tests, but only for two days of measurements. As the modeling's purpose focuses on the system potential, this was considered sufficiently accurate. However, it could be interesting to expand the model in further work to take into account historical weather data for the region where the system is implemented.

Another important modeling detail is that the mass flow is directly controlled to imitate the thermostatic valve. A thermostatic valve will continuously adjust the opening to control the mass flow, while the mass flows were optimized in control intervals of one minute to 20 minutes during simulations. As seen in figure 4.7, the direct mass flow control approaches the behavior of a thermostatic valve for a high number of control intervals. Table 4.4 shows that there is little difference in performance between a high and low number of control intervals. Therefore, the direct mass flow control was concluded to be an accurate enough representation of the thermostatic valve.

5.2 Further Work

Based on the above discussion, the following suggestions are made for further work on the model:

1. End users and geographical areas should be clearly defined before building a final system. This model can then be utilized to optimize the operation for different locations and numbers of people.
2. Models for expected electricity production based on long term weather data could

be developed. The models can be used to create specific strategies for regions with different solar radiation conditions.

3. The model can be expanded to incorporate the system as part of an off-grid PV production system. The demand of electrical appliances with priority over the storage system can be defined and simulated to determine how much excess electricity that will be stored by the three tank system.

6 Conclusion

In this thesis, the operation of a solar powered thermal energy storage system for cooking was optimized. The main objective was to investigate the potential cooking capacity of the system during varying conditions. Alternative designs were also modeled to consider system configurations with potentially enhanced performance.

A challenge with modeling of the system is the uncertainty of some model parameters. The majority of the parameters are physical parameters retrieved from the pilot or determined experimentally. However, heat transfer coefficients of the system relevant for cooking were estimated with more uncertainty. A sensitivity analysis showed that the deviation in the parameters must be large before having large effect on the results.

In terms of size, the current physical pilot is sufficiently large to cook for 100 people when operated optimally. Simulations suggest that increasing the solar panel count from the current number of six to ten will give the system capacity to cook for 100 people twice during a sunny day.

The results indicate that the current manual valve operation for cooking achieves desired performance. If the manual valve used for cooking is operated correctly, the opening must only be adjusted a handful of times during cooking. However, it is recommended to install a thermostatic valve to replace the manual valve, as an excessive flow of only 15 % nearly empties the tank before cooking is finished.

If the system is to be scaled up, a large centralized storage tank could reduce the heat losses. This would increase the energy efficiency or decrease the time required to heat the tank. Although using several smaller systems is less energy efficient, it provides a higher reliability. If one of the small systems break down, the others can still cook during the repair. For a centralized system, all cooking is shut down during maintenance. Other ways of increasing the reliability could be to use fewer and larger heating elements - or by introducing redundant heating elements to ensure functionality even if one or more elements break down.

Besides the scaled up configuration, two modified systems were considered. Adding a second water heating unit after the first stores more energy in water. The second casserole reached a temperature of 58 °C, but the practical benefit of heating the water is small unless a second batch of food is cooked right away. The second modification of removing tank 3 and recycling the oil back to the storage tank could save a significant amount of energy. This could make the system less vulnerable to shifting weather throughout the day, as less energy is required to heat the system a second time.

References

[1] M. Rekdal, *Dynamic Modeling of a Solar Powered Thermal Energy Storage System for Cooking*. Trondheim: Norwegian University of Science and Technology, 2019, p. 31.

[2] British Petroleum Company, *BP Statistical Review of World Energy*. London: British Petroleum Co., 2019, pp. 2–4.

[3] United Nations Economic Commissions for Africa, *2018 Africa Sustainable Development Report: Towards a transformed and resilient continent*. Addis Ababa: United Nations Economic Commissions for Africa, 2018, p. 29.

[4] J. Barbieri, F. Riva, and E. Colombo, "Cooking in refugee camps and informal settlements: A review of available technologies and impacts on the socio-economic and environmental perspective", *Sustainable Energy Technologies and Assessments*, vol. 22, pp. 194–207, Aug. 2017.

[5] P. B. Nielsen, M. Hørmann, J. N. Rud, and F. M. Laugesen, *Renewable energy supply and storage: Guide for planners & developers in sparsely populated areas*. Copenhagen: Nordisk Ministerråd, 2016, p. 39.

[6] P. Sandwell, N. L. A. Chan, S. Foster, D. Nagpal, C. J. M. Emmott, C. Candelise, S. J. Buckle, N. Ekins-Daukes, A. Gambhir, and J. Nelson, "Off-grid solar photovoltaic systems for rural electrification and emissions mitigation in India", *Solar Energy Materials and Solar Cells*, vol. 156, pp. 147–156, 2016.

[7] R. Ooka and S. Ikeda, "A review on optimization techniques for active thermal energy storage control", *Energy and Buildings*, vol. 106, pp. 225–233, 2015.

[8] S. Thaule, M. Kolderup, and K. Gustasfson, *Excess solar, wind, and hydro power to charge heat storage for cooking*. Trondheim: Norwegian University of Science and Technology, 2019, p. 68.

[9] I. Dincer and M. A. Ezan, *Heat Storage: A Unique Solution For Energy Systems*. Cham: Springer International Publishing, 2018, pp. 57–84.

[10] I. Dincer, *Thermal Energy Storage: Systems and Applications*. 2nd ed. London: John Wiley & Sons, 2011, pp. 83–92.

[11] H. Mehling and L. F. Cabeza, *Heat and cold storage with PCM: An up to date introduction into basics and applications*. Berlin, Heidelberg: Springer Berlin Heidelberg, 2008, pp. 1–10.

[12] L. T. Biegler, *Nonlinear Programming*. Philadelphia: Society for Industrial and Applied Mathematics, 2010, p. 399.

[13] M. S. Rana, H. Pota, and I. Petersen, "Performance of sinusoidal scanning with MPC in AFM imaging", *IEEE/ASME Transactions on Mechatronics*, vol. 20, 2014.

[14] J. Jäschke, *Dynamic Optimization for MPC*. Lecture notes, Model Predictive Control, NTNU, delivered 10.09.2019.

[15] A. Høyland, *System reliability theory : models and statistical methods*, 2nd ed., ser. Wiley series in probability and mathematical statistics. New York: John Wiley & Sons, 2004, pp. 15–166.

[16] S. Skogestad, *Prosessteknikk : masse- og energibalanser*, 2. utg. Trondheim: Tapir, 2003, pp. 218–219.

[17] S. Blundell, *Concepts in Thermal Physics*, 2nd ed. Oxford: Oxford University Press, 2010, pp. 99–101.

[18] A. Blackman, *Aylward and Findlay's SI Chemical Data*, 7th ed. Milton: John Wiley & Sons, 2014, p. 176.

[19] Chempro, "Palm Oil Properties", *(Date Accessed: 07.11.2019)*, [Online]. Available: `https://www.chempro.in/palmoilproperties.htm`.

[20] Knovel, "Yaws' Critical Property Data for Chemical Engineers and Chemists - Table 212. Thermal Conductivity - Stainless Steels", *(Date Accessed: 07.11.2019)*, [Online]. Available: `https://app.knovel.com/web/view/itable/show.v/rcid:kpYCPDCECD/cid:kt00AAAHWC/viewerType:eptble//root_slug:table-212-thermal-conductivity---stainless-steels-log-k--a--bt/url_slug:table-212-thermal-conductivity?kpromoter=federation&filter=graph&b-toc-cid=kp`.

[21] Engineers Edge, *Convective Heat Transfer Coefficient Chart*. [Online]. Available: `https://www.engineeringtoolbox.com/convective-heat-transfer-d_430.html`.

[22] J. Andersson, J. Åkesson, and M. Diehl, "Dynamic optimization with CasADi", *2012 IEEE 51st IEEE Conference on Decision and Control (CDC)*, pp. 681–686, Dec. 2012.

[23] Riceland, "Rice Cooking Instructions", *(Date Accessed: 05.02.2020)*, [Online]. Available: `https://www.riceland.com/pages/rice-cooking-instructions/`.

[24] R. C. Hansen, *Overall Equipment Effectiveness: A Powerful Production/maintenance Tool for Increased Profits*. New York: Industrial Press, 2001, pp. 249–250.

Appendices

A Tank 2 Heat Loss Lab Experiment

The temperatures were logged every five seconds and a resulting heat transfer coefficient was calculated, resulting in an excel sheet of 17 000 + rows. Selected results at key times are given below:

Table A.1: Temperature in tank 2, total heat $\hat{Q}_{2R}$ over time, and calculated average heat transfer coefficient of the tank during the experiment

Time [h]	T_2 [K]	Total $\hat{Q}_{2R}$ [MJ]	$U_2[W/m^2K]$
0	226.13	0.000	-
1	212.10	0.268	2.02
2	199.48	0.508	2.13
4	175.87	0.960	2.15
6	156.41	1.330	2.12
12	113.23	2.150	2.04
24	66.61	3.040	1.92

B Additional MATLAB Plots

Below are MATLAB plots including all system states. The plots are included for instances where systems states were omitted from the main report figures to illustrate only important features.

B.1 Weather Variations - Cloudy Weather Max Temperature

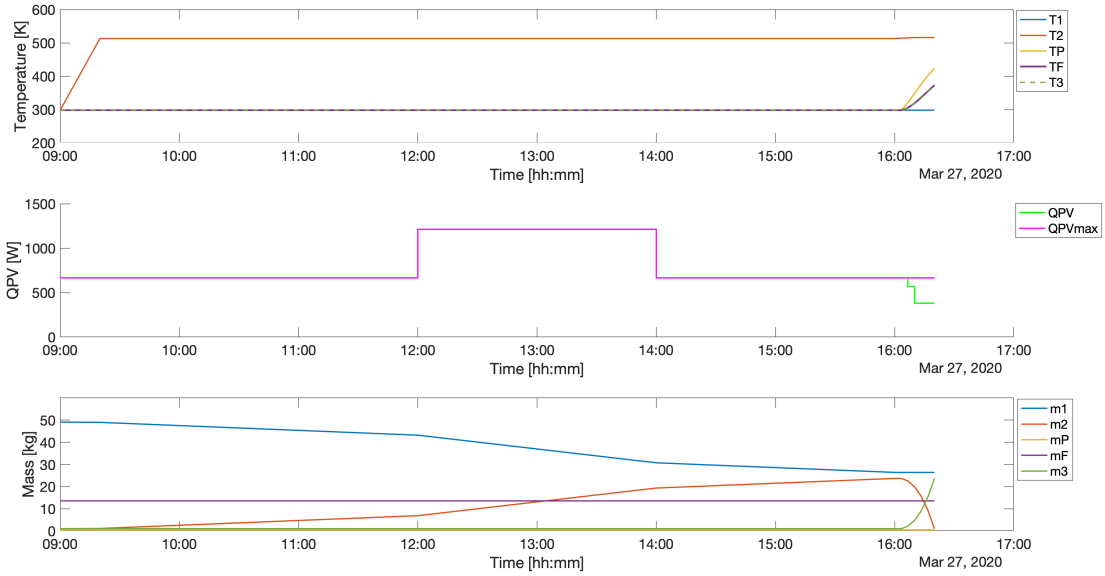

Figure B.1: System states and solar input during a day of cloudy weather. Top to bottom: 1. Temperatures in the control volumes 2. Solar power input available, $\hat{Q}_{PV,max}$ and used, $\hat{Q}_{PV}$. 3. Mass in the control volumes.

B.2 Weather Variations - Cloudy Weather Max Level

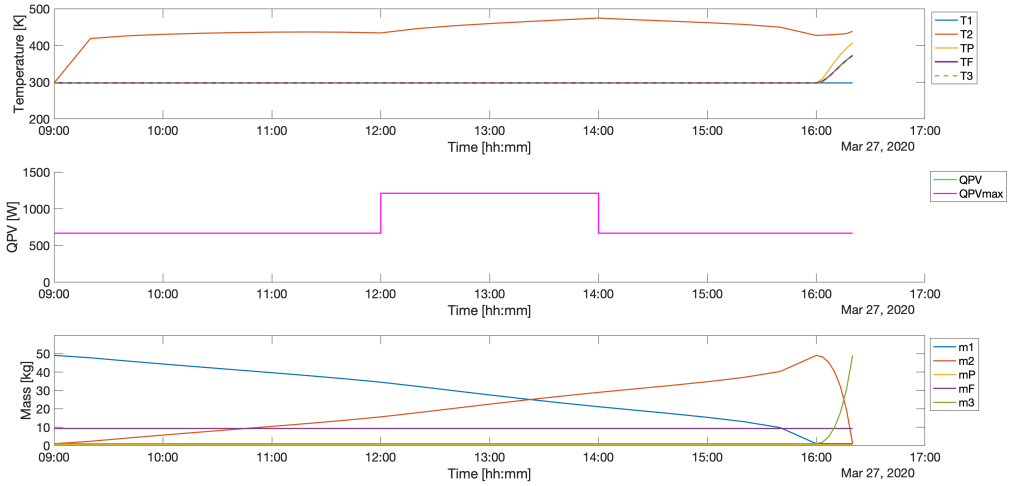

Figure B.2: System states and solar input during a day of cloudy weather. Top to bottom: 1. Temperatures in the control volumes 2. Solar power input available, $\hat{Q}_{PV,max}$ and used, $\hat{Q}_{PV}$. 3. Mass in the control volumes.

B.3 System Modification Study - Additional PF Unit

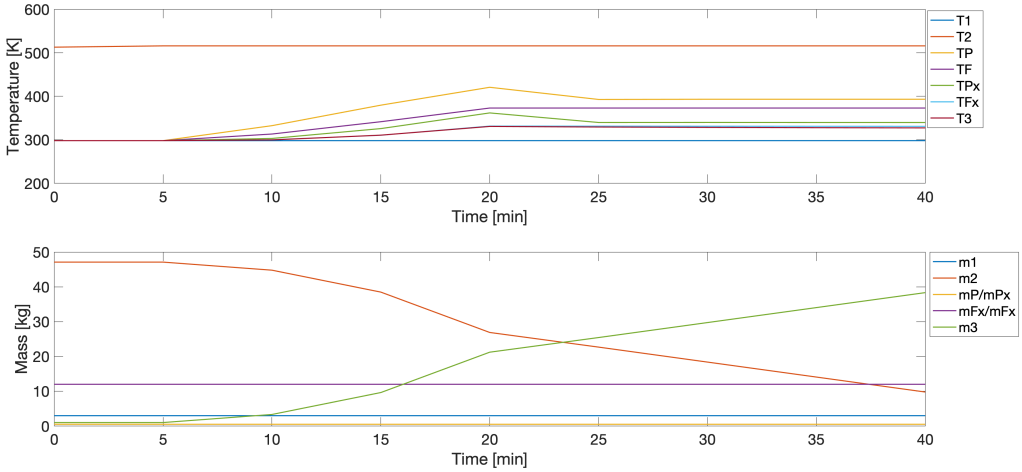

Figure B.3: System states and solar input during a day of sunny weather. Top: Temperatures in the control volumes. Bottom: Mass in the control volumes.

B.4 System Modification Study - Two Tank System

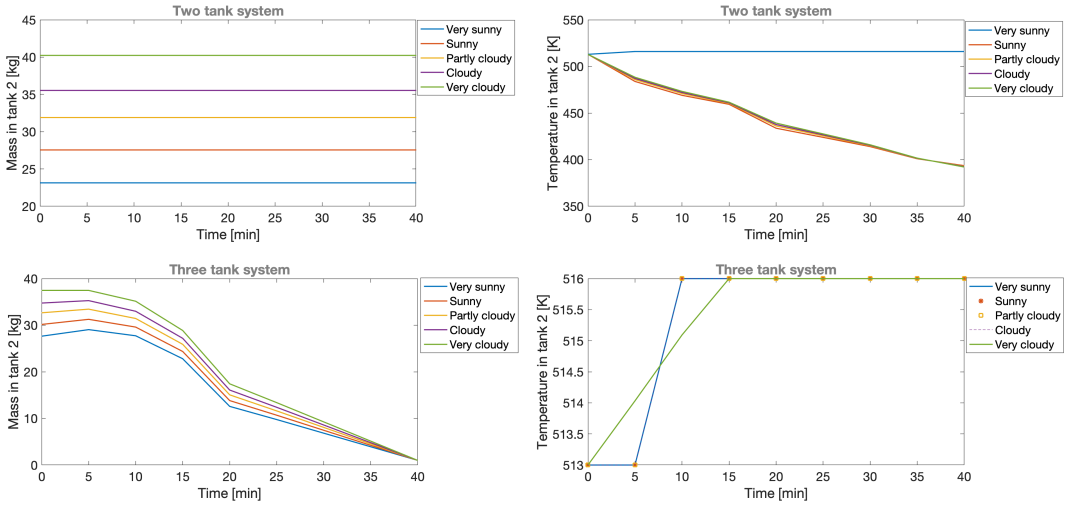

Figure B.4: Top: system masses and temperatures during cooking with minimal initial mass in the modified two tank system. Bottom: system masses and temperatures during cooking with minimal initial mass in the original three tank system.

C MATLAB Codes

Below are samples of the MATLAB codes used for the various case studies. The complete collection of scripts were provided as an attachment to the thesis submission.

C.1 Study 1 - Size Optimization

```
%% Study 1 – Tank size optimization
clear
addpath('/Users/Mikal/Documents/MATLAB/casadi-osx-matlabR2015a-v3.4.5')
import casadi.*
addpath('/Users/Mikal/Documents/MATLAB/Masteroppgave/Final Simulations')

SystemParameters;

clearvars Ltank Dtank Atankend Vtank Tanksurface;

% Optimization parameters
T = 1800; % simulation time, from 1500 – 2400 [s]
N = 6; % number of control intervals, from 5 – 8
limdiv = 1; % when to change water temperature limit, from 0 – 3
MFmass = 12; % water mass, from 3 – 20 [kg]
nu = 4; % number of control inputs
ns = 10; % number of states
TFlowerlim = [298*ones(limdiv,1); 373*ones(N-limdiv,1)]; % lower limit TF

% System declaring variables
T1 = SX.sym('T1');
T2 = SX.sym('T2');
TP = SX.sym('TP');
TF = SX.sym('TF');
T3 = SX.sym('T3');
M1 = SX.sym('M1');
M2 = SX.sym('M2');
MP = SX.sym('MP');
MF = SX.sym('MF');
M3 = SX.sym('M3');
x = [T1;T2;TP;TF;T3;M1;M2;MP;MF;M3];
u1 = SX.sym('QPV');
u2 = SX.sym('Dtank');
u3 = SX.sym('Ltank');
u4 = SX.sym('m2p');
u = [u1;u2;u3;u4];

```

```
% Transport equations
Ltank = u3; % tank length
Atankend = pi*u2^2/4; % tank end area
Vtank = Atankend*Ltank; % Volume of tank
Tanksurface = 2*Atankend + 2*pi*(u2/2)*u3; % tank surface area
m12 = 0;
m2p = u4;
mp3 = m2p;
m31 = 0;

Q1R = f*U*Tanksurface*(T1-To);
Q2R = U*Tanksurface*(T2-To);
Q3R = f*U*Tanksurface*(T3-To);
QPF = hpf*APF*(TP-TF);
QPR = hpr*APR*(TP-To);
QFR = hfr*AFR*(TF-To);

% model equations
xdot = [(1/M1)*(m31*(T3-T1)-Q1R/cp);
         (1/M2)*(u1/cp+m12*(T1-T2)-Q2R/cp);
         (1/MP)*(m2p*(T2-TP)-QPF/cp-QPR/cp);
         (1/MF)*(QPF/cpw-QFR/cpw);
         (1/M3)*(mp3*(TP-T3)-Q3R/cp);
         m31-m12;
         m12-m2p;
         0;
         0;
         mp3-m31];

% Objective term
L = pi*(u2^2/4)*u3; % minimize tank size

% Continuous time dynamics
f = Function('f', {x, u}, {xdot, L});

% CVODES from the SUNDIALS suite
dae = struct('x',x,'p',u,'ode',xdot,'quad',L);
opts = struct('tf',T/N);
F = integrator('F', 'cvodes', dae, opts);

% Start with an empty NLP
w={};
w0 = [];
lbw = [];
ubw = [];
J = 0;
```

```
84  g={};
85  lbg = [];
86  ubg = [];
87
88  % "Lift" initial conditions
89  Xk = MX.sym('X0', 10);
90  w = {w{:}, Xk};
91  lbw = [lbw; 298; 513; 298; 298; 298; 1; 10; 0.5; MFmass; 1];
92  ubw = [ubw; 298; 513; 298; 298; 298; 1; 300; 0.5; MFmass; 1];
93  w0 = [w0; 298; 513; 298; 298; 298; 1; 300; 0.5; MFmass; 1];
94
95  % Formulate the NLP
96
97  for k=0:N-1
98
99      % State constraints
100     lbwt = [298; 513; 373; TFlowerlim(k+1); 298; 1; 10; 0.5; MFmass; 1];
101     ubwt = [516; 516; 516; 378; 516; 300; 300; 1; 20; 300];
102     w0t = [298; 513; 513; 373; 298; 1; 30; 0.5; MFmass; 30];
103
104     Uk = MX.sym(['U_' num2str(k)], nu);
105     w = {w{:}, Uk};
106
107     % Save optimal sizes
108     if k == 0
109         Uk_2 = Uk(2);
110         Uk_3 = Uk(3);
111     end
112
113     % Control input constraints
114     lbw = [lbw; 0; 0.3; 0.3; 0];
115     ubw = [ubw; 2639; 1; 0.7; 1];
116     w0 = [w0;  400.4; 0.7; 0.3; 0.0143];
117
118     % Additional constraints - tanks 2 and 3 cannot be overfilled
119     g = [g, {Uk(3)*pi*(Uk(2))^2/4-Xk(7)/rho}, ...
            {Uk(3)*pi*(Uk(2))^2/4-Xk(10)/rho}];
120     lbg = [lbg; 0; 0];
121     ubg = [ubg; inf; inf];
122
123     % Integrate till the end of the interval
124     Fk = F('x0', Xk, 'p', Uk);
125     Xk_end = Fk.xf;
126
127     % New NLP variable for state at end of interval
128     Xk = MX.sym(['X_' num2str(k+1)], 10);
```

```
129       w = [w, {Xk}];
130       lbw = [lbw; lbwt];
131       ubw = [ubw;  ubwt];
132       w0 = [w0;w0t];
133
134       % Add equality constraint
135       g = [g, {Xk_end-Xk}];
136       lbg = [lbg; 0; 0; 0; 0; 0; 0; 0; 0; 0; 0];
137       ubg = [ubg; 0; 0; 0; 0; 0; 0; 0; 0; 0; 0];
138
139       % Dtank and Ltank must be kept constant
140       dUk = [Uk(2)-Uk_2; Uk(3)-Uk_3];
141       g = {g{:}, dUk};
142       lbg = [lbg; 0; 0];
143       ubg = [ubg; 0; 0];
144
145   end
146
147   J = Uk(3)*pi*Uk(2)^2/4;
148
149   % Create an NLP solver
150   prob = struct('f', J, 'x', vertcat(w{:}), 'g', vertcat(g{:}));
151   solver = nlpsol('solver', 'ipopt', prob);
152
153   % Solve the NLP
154   sol = solver('x0', w0, 'lbx', lbw, 'ubx', ubw,...
155                'lbg', lbg, 'ubg', ubg);
156   w_opt = full(sol.x);
```

C.2 Study 2.2 Weather Variations - Sunny Heating

```
1   %% Sunny weather heating
2
3   clear
4   addpath('/Users/Mikal/Documents/MATLAB/casadi-osx-matlabR2015a-v3.4.5')
5   import casadi.*
6   addpath('/Users/Mikal/Documents/MATLAB/Masteroppgave/Final Simulations')
7   SystemParameters;
8
9   % Optimization parameters
10  T = 3600*3; % Time horizon
11  N = 9; % number of control intervals
12  nu = 3; % number of controls
13  QPVlim = [2132*ones(1,3), 2639*ones(1,6)]; % max solar input
```

```
14
15 % System declaring variables
16 T1 = SX.sym('T1');
17 T2 = SX.sym('T2');
18 TP = SX.sym('TP');
19 TF = SX.sym('TF');
20 T3 = SX.sym('T3');
21 M1 = SX.sym('M1');
22 M2 = SX.sym('M2');
23 MP = SX.sym('MP');
24 MF = SX.sym('MF');
25 M3 = SX.sym('M3');
26 x = [T1;T2;TP;TF;T3;M1;M2;MP;MF;M3];
27 u1 = SX.sym('QPV');
28 u2 = SX.sym('m12');
29 u3 = SX.sym('m2p');
30 u = [u1;u2;u3];
31
32 % Transport equations
33 m12 = u2;
34 m31 = 0;
35 m2p = 0;
36 mp3 = m2p;
37
38 Q1R = f*U*Tanksurface*(T1-To);
39 Q2R = U*Tanksurface*(T2-To);
40 Q3R = f*U*Tanksurface*(T3-To);
41 QPF = hpf*APF*(TP-TF);
42 QPR = hpr*APR*(TP-To);
43 QFR = hfr*AFR*(TF-To);
44
45   % model equations
46   xdot = [(1/M1)*(m31*(T3-T1)-Q1R/cp);
47        (1/M2)*(u1/cp+m12*(T1-T2)-Q2R/cp);
48        (1/MP)*(m2p*(T2-TP)-QPF/cp-QPR/cp);
49        (1/MF)*(QPF/cpw-QFR/cpw);
50        (1/M3)*(mp3*(TP-T3)-Q3R/cp);
51        m31-m12;
52        m12-m2p;
53        0;
54        0;
55        mp3-m31];
56
57 % Objective term
58  L = -M2; % maximize mass in tank 2
59
```

```
% Continuous time dynamics
f = Function('f', {x, u}, {xdot, L});

% CVODES from the SUNDIALS suite
dae = struct('x',x,'p',u,'ode',xdot,'quad',L);
opts = struct('tf',T/N);
F = integrator('F', 'cvodes', dae, opts);

% Start with an empty NLP
w={};
w0 = [];
lbw = [];
ubw = [];
J = 0;
g={};
lbg = [];
ubg = [];

% Initial conditions in the morning
T10 = 298; T20 = 298; TP0 = 298; TF0 = 298;
T30 = 298; M10 = 49.1; M20 = 1; M30 = 1;
MP0 = 0.5; MF0 = 12;

%% Initial conditions for heating after lunch and pumping:
% load('SunnyPumping','T1_opt','T2_opt','TP_opt','TF_opt','T3_opt',...
% 'M1_opt','M2_opt','MP_opt','MF_opt','M3_opt','u1_opt','u2_opt','u3_opt')
%
% T10 = T1_opt(end); T20 = T2_opt(end); TP0 = TP_opt(end); TF0 = TF_opt(end);
% T30 = T3_opt(end); M10 = M1_opt(end); M20 = M2_opt(end); M30 = M3_opt(end);
% MP0 = MP_opt(end); MF0 = MF_opt(end);

% "Lift" initial conditions
Xk = MX.sym('X0', 10);
w = {w{:}, Xk};
lbw = [lbw; T10; T20; TP0; TF0; T30; M10; M20; MP0; MF0; M30];
ubw = [ubw; T10+eps; T20+eps; TP0+eps; TF0+eps; T30+eps; M10+eps; ...
    M20+eps; MP0+eps; MF0+eps; M30+eps];
w0 = [w0; T10; T20; TP0; TF0; T30; M10; M20; MP0; MF0; M30];

% Formulate the NLP
for k=0:N-1

    lbwt = [298; 513; 298; 298; 298; 1; 1; 0.5; 12; 1];
    ubwt = [516; 516; 516; 378; 516; 49.1; 49.1; 1; 15; 49.1];
    w0t = [298; 513; 298; 298; 298; 20; 20; 0.5; 12; eps];

```

```
105      Uk = MX.sym(['U_' num2str(k)], nu);
106      w = {w{:}, Uk};
107
108      lbw = [lbw; 0; 0; 0];
109      ubw = [ubw; QPVlim(k+1); 1; 0];
110      w0 = [w0; QPVlim(k+1)/2; 0.002; 0];
111
112      % Integrate till the end of the interval
113      Fk = F('x0', Xk, 'p', Uk);
114      Xk_end = Fk.xf;
115      % J=J+Fk.qf;
116
117      % New NLP variable for state at end of interval
118      Xk = MX.sym(['X_' num2str(k+1)], 10);
119      w = [w, {Xk}];
120      lbw = [lbw; lbwt];
121      ubw = [ubw;  ubwt];
122      w0 = [w0;w0t];
123
124      % Add equality constraint
125      g = [g, {Xk_end-Xk}];
126      lbg = [lbg; 0; 0; 0; 0; 0; 0; 0; 0; 0; 0];
127      ubg = [ubg; 0; 0; 0; 0; 0; 0; 0; 0; 0; 0];
128
129  end
130
131  J = -Xk(7);
132
133  % Create an NLP solver
134  prob = struct('f', J, 'x', vertcat(w{:}), 'g', vertcat(g{:}));
135  solver = nlpsol('solver', 'ipopt', prob);
136
137  % Solve the NLP
138  sol = solver('x0', w0, 'lbx', lbw, 'ubx', ubw,...
139               'lbg', lbg, 'ubg', ubg);
140  w_opt = full(sol.x);
```

C.3 Study 2.2 Weather Variations - Sunny Cooking

```
1  %% Sunny weather cooking
2
3  clear
4  addpath('/Users/Mikal/Documents/MATLAB/casadi-osx-matlabR2015a-v3.4.5')
5  import casadi.*
```

```
addpath('/Users/Mikal/Documents/MATLAB/Masteroppgave/Final Simulations')
SystemParameters;

% Optimization parameters
T = 2400; % simulation time, from 1500 - 2400 [s]
N = 8; % control intervals
nu = 3; % number of controls
limdiv = 3; % when to change water temperature limit, from 0 - 3
TFlowerlim = [298*ones(limdiv,1); 373*ones(N-limdiv,1)]; % lower limit TF
QPVlim = [2639*ones(1,N)]; % max solar input

% System declaring variables
T1 = SX.sym('T1');
T2 = SX.sym('T2');
TP = SX.sym('TP');
TF = SX.sym('TF');
T3 = SX.sym('T3');
M1 = SX.sym('M1');
M2 = SX.sym('M2');
MP = SX.sym('MP');
MF = SX.sym('MF');
M3 = SX.sym('M3');
x = [T1;T2;TP;TF;T3;M1;M2;MP;MF;M3];
u1 = SX.sym('QPV');
u2 = SX.sym('m12');
u3 = SX.sym('m2p');
u = [u1;u2;u3];

% Transport equations
m12 = u2;
m31 = 0;
m2p = u3;
mp3 = m2p;

Q1R = f*U*Tanksurface*(T1-To);
Q2R = U*Tanksurface*(T2-To);
Q3R = f*U*Tanksurface*(T3-To);
QPF = hpf*APF*(TP-TF);
QPR = hpr*APR*(TP-To);
QFR = hfr*AFR*(TF-To);

% model equations
xdot = [(1/M1)*(m31*(T3-T1)-Q1R/cp);
    (1/M2)*(u1/cp+m12*(T1-T2)-Q2R/cp);
    (1/MP)*(m2p*(T2-TP)-QPF/cp-QPR/cp);
    (1/MF)*(QPF/cpw-QFR/cpw);
```

```
52      (1/M3)*(mp3*(TP-T3)-Q3R/cp);
53      m31-m12;
54      m12-m2p;
55      m2p-mp3;
56      0;
57      mp3-m31];
58
59  % Objective term
60   L = u3; % minimize total mass flow used
61
62  % Continuous time dynamics
63  f = Function('f', {x, u}, {xdot, L});
64
65     % CVODES from the SUNDIALS suite
66     dae = struct('x',x,'p',u,'ode',xdot,'quad',L);
67     opts = struct('tf',T/N);
68     F = integrator('F', 'cvodes', dae, opts);
69
70  % Start with an empty NLP
71  w={};
72  w0 = [];
73  lbw = [];
74  ubw = [];
75  J = 0;
76  g={};
77  lbg = [];
78  ubg = [];
79
80  %% Initial conditions when cooking for lunch:
81  % load('HeatingSunnyMorning','T1_opt','T2_opt','TP_opt','TF_opt','T3_opt',...
82  % 'M1_opt','M2_opt','MP_opt','MF_opt','M3_opt','u1_opt','u2_opt','u3_opt')
83
84  %% Initial conditions when cooking for dinner:
85  load('HeatingSunnyAfternoon','T1_opt','T2_opt','TP_opt','TF_opt','T3_opt',...
86  'M1_opt','M2_opt','MP_opt','MF_opt','M3_opt','u1_opt','u2_opt','u3_opt')
87
88  T10 = T1_opt(end); T20 = T2_opt(end); TP0 = TP_opt(end); TF0 = TF_opt(end);
89  T30 = T3_opt(end); M10 = M1_opt(end); M20 = M2_opt(end); M30 = M3_opt(end);
90  MP0 = MP_opt(end); MF0 = MF_opt(end);
91
92  % % "Lift" initial conditions
93  Xk = MX.sym('X0', 10);
94  w = {w{:}, Xk};
95  lbw = [lbw; T10; T20; TP0; TF0; T30; M10; M20; MP0; MF0; M30];
96  ubw = [ubw; T10+eps; T20+eps; TP0+eps; TF0+eps; T30+eps; M10+eps; ...
        M20+eps; MP0+eps; MF0+eps; M30+eps];
```

```
97  w0 = [w0; T10; T20; TP0; TF0; T30; M10; M20; MP0; MF0; M30];
98
99  % Formulate the NLP
100
101 for k=0:N-1
102
103     lbwt = [298; 513; 298; TFlowerlim(k+1); 298; 1; 1; 0.5; 12; 1];
104     ubwt = [516; 516; 516; 378; 516; 49.1; 49.1; 1; 15; 49.1];
105     w0t = [298; 513; 513; 298; 298; 20; 20; 0.5; 12; 20];
106
107     Uk = MX.sym(['U_' num2str(k)], nu);
108     w = {w{:}, Uk};
109
110     lbw = [lbw; 0; 0; 0];
111     ubw = [ubw; QPVlim(k+1); 0; 1];
112     w0 = [w0; 0; 0; 0.02];
113
114     % Integrate till the end of the interval
115     Fk = F('x0', Xk, 'p', Uk);
116     Xk_end = Fk.xf;
117     J=J+Fk.qf;
118
119     % New NLP variable for state at end of interval
120     Xk = MX.sym(['X_' num2str(k+1)], 10);
121     w = [w, {Xk}];
122     lbw = [lbw; lbwt];
123     ubw = [ubw;  ubwt];
124     w0 = [w0;w0t];
125
126     % Add equality constraint
127     g = [g, {Xk_end-Xk}];
128     lbg = [lbg; 0; 0; 0; 0; 0; 0; 0; 0; 0; 0];
129     ubg = [ubg; 0; 0; 0; 0; 0; 0; 0; 0; 0; 0];
130
131 end
132
133 % Create an NLP solver
134 prob = struct('f', J, 'x', vertcat(w{:}), 'g', vertcat(g{:}));
135 solver = nlpsol('solver', 'ipopt', prob);
136
137 % Solve the NLP
138 sol = solver('x0', w0, 'lbx', lbw, 'ubx', ubw,...
139             'lbg', lbg, 'ubg', ubg);
140 w_opt = full(sol.x);
```

D Field Test Effect Data

The data below are recorded measurements from field tests performed in Arusha in March 2019 by Thaule et.al (2019) as part of their master's thesis work [8]. The raw data was not included in their report, but was provided upon request for this thesis and translated from Norwegian to English by the author of this paper.

Table D.1: Field Test 14.03.2019

Time	Voltage [V]	T_2 [°C]	Effect [W]	Weather Conditions
11:00	206.0	66.0	947.6	Partly cloudy
11:10	205.4	75.0	965.4	Partly sunny
11:20	206.6	84.0	991.7	Partly sunny
11:30	206.5	94.8	991.2	Partly sunny
11:40	206.3	103.3	969.6	Partly sunny
11:50	205.0	113.0	82.0	Very cloudy during measurement
12:00	205.4	119.0	1006.5	
12:10	204.5	129.3	1124.8	
12:20	204.0	136.3	1081.2	
12:30	203.3	143.3	1118.2	Partly cloudy
12:40	203.7	150.5	977.8	Partly cloudy
12:50	204.0	157.3	1060.8	Partly cloudy
13:00	204.4	162.8	1165.1	Partly cloudy
13:10	204.2	171.5	1174.2	
13:20	203.9	176.5	1076.6	
13:30	204.0	183.8	1081.2	
13:40	204.1	189.8	1081.7	
13:50	204.5	196.3	1053.2	
14:00	203.9	200.5	999.1	
14:10	203.3	206.3	1146.6	
14:20	196.6	212.0	884.7	Cloudy
14:30	204.6	217.3	1023.0	
14:40	203.6	221.3	965.1	
14:50	191.0	227.0	888.2	Cloudy
15:00	203.5	231.0	970.7	Cloudy
15:10	204.5	234.8	920.3	Cloudy
15:20	203.8	238.5	892.6	Cloudy
15:30	204.1	243.8	867.4	Cloudy

Table D.2: Field Test 15.03.2019

Time	Voltage [V]	T_2 [°C]	Effect [W]	Weather Conditions
09:20	225.5	69.3	135.3	Cloudy
09:30	222.1	72.5	133.3	Cloudy
09:40	225.0	76.3	1372.5	Partly sunny
09:50	225.4	78.8	137.5	
10:00	223.0	85.0	1583.3	Sunny
10:10	218.0	91.5	1504.2	Sunny
10:20	221.1	101.5	884.4	Partly cloudy
10:30	208.7	110.0	1273.1	
10:40	211.0	122.8	844.0	Cloudy
10:50	206.6	135.3	1183.8	
11:00	206.1	146.5	1226.3	
11:10	205.4	158.8	1119.4	
11:20	204.5	169.5	1104.3	Partly cloudy
11:30	204.3	180.0	1123.7	Sunny
11:40	204.1	190.8	1102.1	Sunny
11:50	203.5	199.5	1098.9	
12:00	204.1	208.5	1081.7	Sunny
12:10	204.3	217.5	1148.2	
12:20	204.0	226.0	1101.6	
12:30	204.3		1103.2	
12:40	204.3		1184.7	
12:50	204.3		1184.7	
13:00	204.3		1184.7	
13:10	204.2		1266.0	
13:20	204.0	243.0	1152.6	
13:30	203.8	236.5	1108.7	
13:40			0	
13:50			0	
14:00			0	
14:10			0	
14:20				
14:30				
14:40				
14:50				

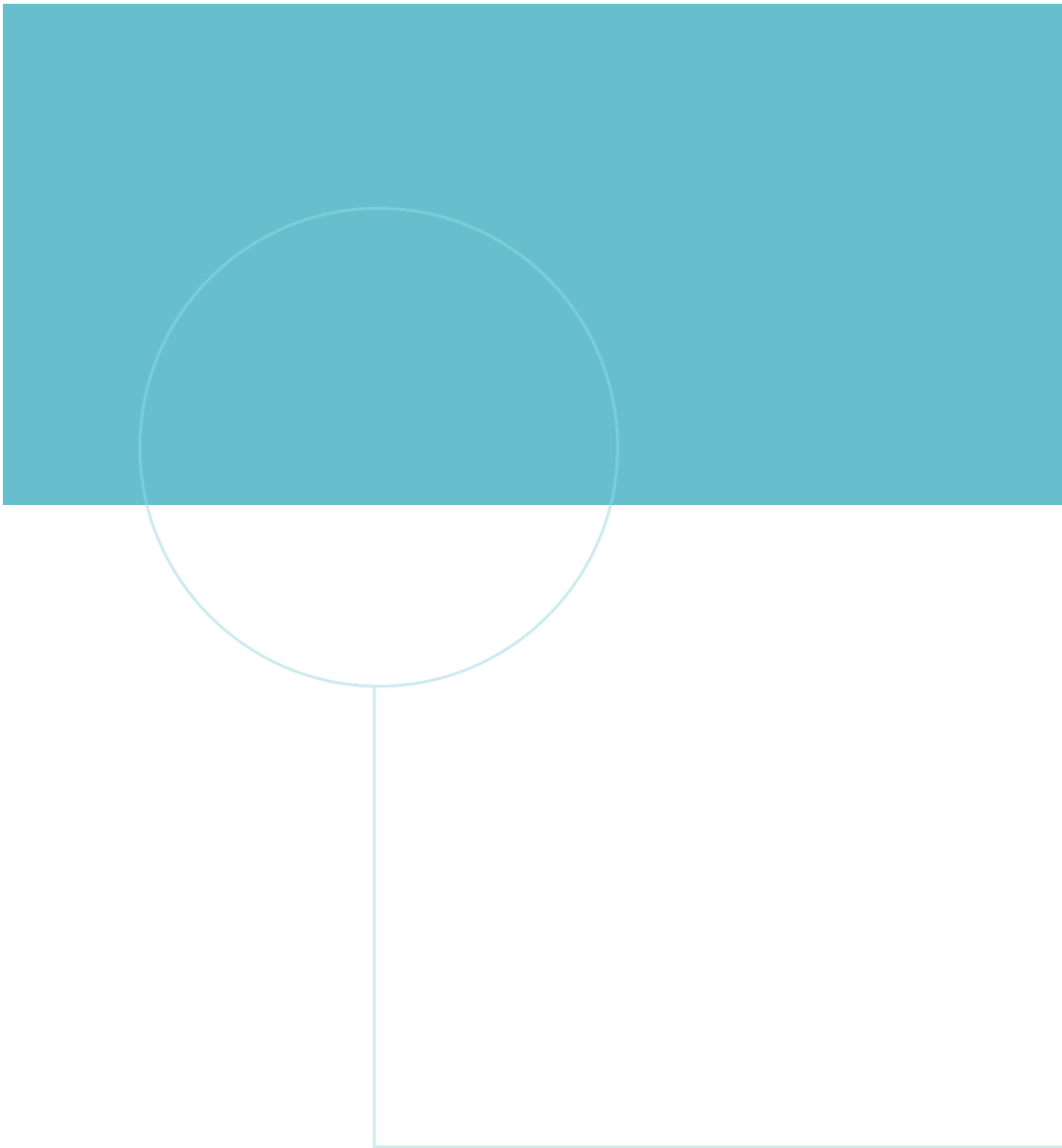

NTNU

Norwegian University of
Science and Technology